UNIVERSITY *of the*
WESTERN CAPE

RESERVOIR HETEROGENEITY OF THE SANDSTONE RESERVOIRS WITHIN THE PLETMOS BASIN, BLOCK11A, OFFSHORE SOUTH AFRICA

A mini thesis in Petroleum Geoscience

*By **NEHEMIAH ELIEZER DOMINICK***

Submitted in partial fulfilment of the requirements for the degree of Magister Scientiae (MSc) in the Faculty of Science, Earth Sciences Department University of the Western Cape, Bellville, South Africa.

Supervisor: Dr. M. Opuwari

Co-supervisor: Prof. J. Van Bever Donker

ABSTRACT

The Pletmos basin throughout its synrift I lower Cretaceous period was influenced by siliciclastic depositional systems. This study is aimed at illustrating the reservoir heterogeneity in the BCII - BCI interval of the Ga-field, offshore South Africa. This was achieved by generating a conceptual static model as a predictive tool for the BCII - BCI interval.

The reservoir zones between BCII - BCI were sub divided into two major zones, viz: zone A and zone B. Petrophysical analysis was conducted on the three wells Ga-A3, Ga-Q1 and Ga-Q2. The application of the sequential gaussian algorithm ensured that all of the available data was honoured to the highest extent in generating the realisations to display the heterogeneity of the BCII – BCI sandstone reservoir. Sampling values from the well logs were extrapolated into the 3D grid. Each reservoir contained a percentage of shale or clay of about 45% -50%. Small scaled reservoir heterogeneity has been construed to the influence of the sedimentary structures. Large scaled reservoir heterogeneity has been identified, due to the lateral extent of the claystones which is widely distributed throughout the study area.

KEYWORDS

Reservoir

Heterogeneity

Pletmos basin

Porosity

Permeability

Upscaling

Facies modelling

Petrophysical modelling

DECLARATION:

I declare that the **Reservoir Heterogeneity of the Sandstone Reservoirs within the Pletmos Basin, Block11a, Offshore South Africa** is my own work that it has not been submitted before for any degree or examination in any other university, and that all the sources I have used or quoted have been indicated and acknowledged by means of complete references.

Nehemiah Dominick **May 2014**

Signed:……

DEDICATION

This project is dedicated to

The

ALMIGHTY GOD

For

I can do all things through Christ who strengthens me.

ACKNOWLEDGEMENT

I would to like give the author and finisher of my faith the Lord Jesus Christ, all the praise, glory and honour. It is only through His grace and mercy that has sustained me through the trials that was encountered throughout this voyage.

It would not have been possible to have written this thesis without the support of my principal supervisor, Dr. M. Opuwari, for his guidance and unsurpassed knowledge of the petroleum field. The support of my co-supervisor Prof. J. Van Bever Donker has been invaluable. To Dr. R. Rutten and Dr. S. Lanes I thank you for the great inspiration that you are and I will cherish the advice and knowledge that was imparted throughout this study.

I am particularly grateful to my parents Mr and Mrs Dominick for the opportunity they could have given me to develop my academic career, for the values that they have instilled in me, their prayers and unequivocal support in all of my endeavours, my mere expression of saying thank you is only a small token of my appreciation for you. To my brothers Micah, Yowceph and sister in-law Ruth for their encouragement and continuous believe in me.

The contribution from the Petroleum Agency of South Africa (PASA) for providing the data that was used in this thesis and their assistance. To Schlumberger I would like to thank the software support team for their assistance it is highly appreciated and well acknowledged.

To my fellow postgraduate students of the Department of Earth Science at the University of the Western Cape, thank you for the time we could of shared and the experiences we could of drawn from one another.

Contents

List of Figures

List of Tables

Preamble

"Production trends are controlled by the complex reservoir sandstone geometry and faults, and discrete compartments are interpreted from the reservoir architecture, structure and trends in oil and water production." (Douglas, et al., 1992).

A rock with sufficient porosity and permeability should be considered a reservoir. If the pores are saturated with water the reservoir is called an aquifer. This is in contrast to a rock with low permeability. It can sometimes block the cross formational fluid transfer and form a barrier to gas and fluid flow; hence it becomes an effective seal (Marty, et al., 2003). "Additionally fractured basement rocks are potential reservoirs, if containing commercial hydrocarbons "(Petford and Mc Caffrey, 2003).

The accurate definition of reservoir architecture and distribution of reservoir facies plays a vital role in determining the characteristics of reservoirs. "A reservoir heterogeneity study is conducted to understand the shale and the sand distribution" (Schlumberger, 2006).

The availability of seismic and well data as well the integration of computer applications assists in the efficiency of the construction of a consistent geological model of the reservoir, using an advanced technology is more feasible based on their interpretation and their integration (Tetyukhina, 2010).

Chapter 1

1.1 Introduction

Accurate predictions of siliciclastic reservoirs are often required in the petroleum industry and such predictions are performed by geoscientists who analyse the geological data that is often sparsely distributed or incomplete. The geological data is used to generate a 3D geological model which comprises a 3D representation of all the elements (shape and volume) as well as the distribution of the reservoir properties. These elements are defined by the reservoir architecture, the properties of the lithofacies and the distribution of porosity and permeability both vertically and laterally. Representatives of the reservoir for this study are taken from core samples, well logs and seismic data.

According to Johnson and Greenkorn (1963), an increase in reliance on physical and digital models in petroleum studies has emphasised that a study of reservoir heterogeneity must identify features of the reservoir which influence its flow parameters such as porosity and permeability. Including geostatistics in such a model is imperative for creating an integrative description of the reservoir. "It is important to consider how the heterogeneity differs on different scales, and this affects the results of reservoir simulations" (McCarthy, 1991).

"Generating a 3D model with sparsely distributed geological data sets naturally results in some uncertainty. Quantifying this uncertainty is important because geological framework models are often used for assessments and decisions that have social and commercial implications" (Bond, et al., 2007).

Quantification of uncertainty in geological models has been acknowledged by various authors including (Aguilera, 2004), for petrophysical models. Understanding the use of geostatistics is essential when understanding the limitations of the tool and acknowledging that interpretation of it also contains a possible uncertainty, but that it is still possible to quantify the heterogeneity that is contained within the reservoir interval.

The BCII- BCI interval, a late Berrasian to early Valanginian synrift shallow marine unit, is an important reservoir interval that was targeted during the exploration for hydrocarbons in the southern portion of the Pletmos basin, offshore South Africa.

1.2 Exploration activity in the Pletmos Basin

According to the Petroleum Agency of South Africa, the exploration for hydrocarbons was initiated in 1940 by the Geological Survey of South Africa. During 1967 a new mining rights act was passed which allowed a number of international oil companies (Total, Gulf Oil, Esso, Shell, Arco, CFP and Superior) to obtain offshore concessions (PASA, 2013). In 1968 the first offshore well was drilled by the Superior Oil Company. The Superior Oil Company also made a discovery of gas and condensate in the lower Cretaceous, synrift shallow marine sandstones in the Ga-A1 well, Block 11a, as highlighted in the figure below, which is situated in the Southern region of the Pletmos Basin. (PASA, 2013).

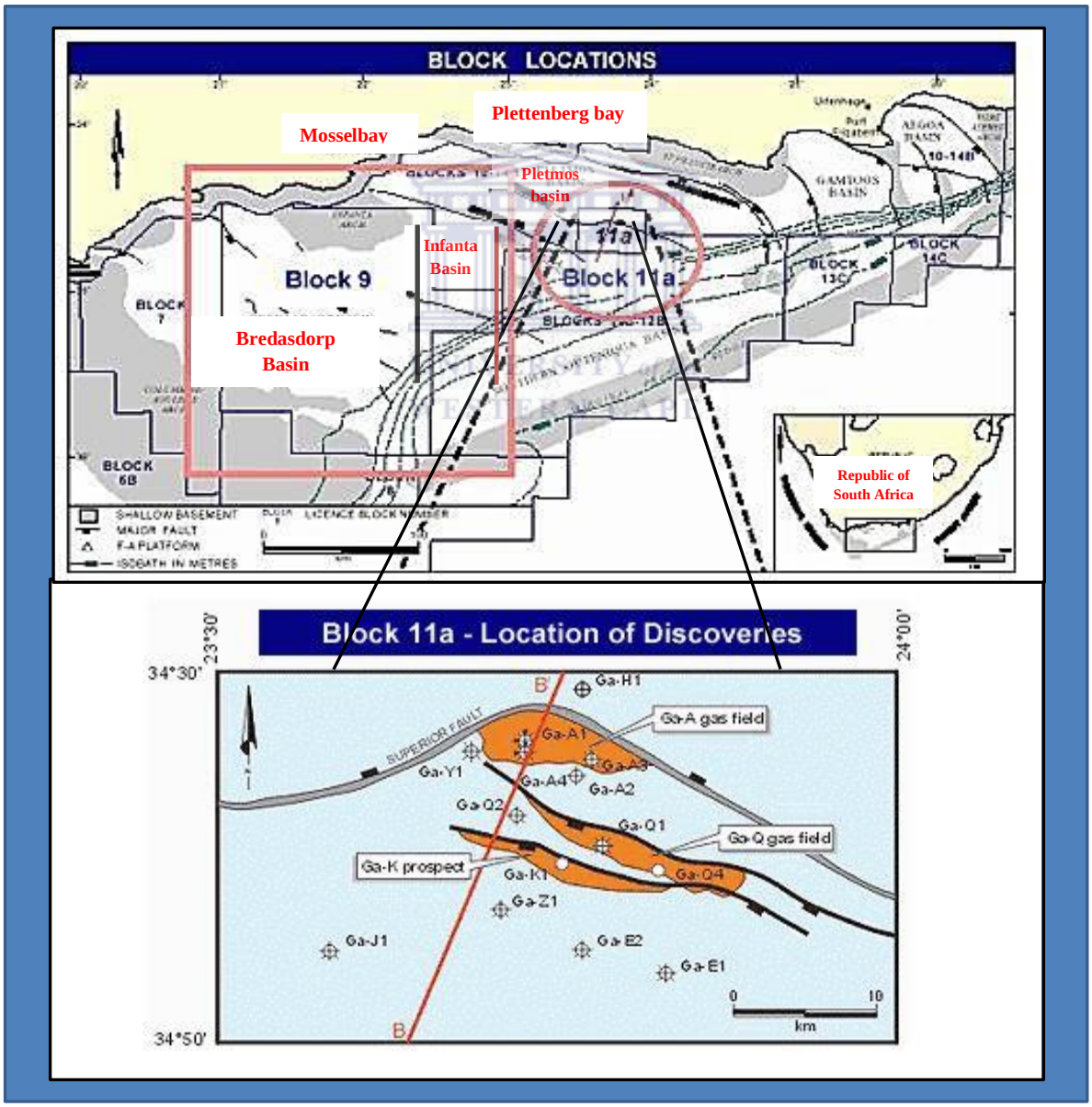

Figure 1.2.1: Block locations of the Pletmos and Bredasdorp sub-basins off the coast of South Africa, modified after (Roux, 1997).

The Well Ga-A1 produced mostly gas at commercial rates of 22MMscfd from the synrift shallow marine sandstones (Roux, 1997). A total of 38 wildcats have been drilled throughout Pletmos basin and the Infanta embayment (figure 1.2.1) the targets were the synrift structures (Roux, 1997). Sandstones at depths of 1565 -2500m had porosities of up to 25% averaging between 11% to 18% and permeabilities which range between 10 and 100mD. (Roux, 1997).

Wells Ga-Q1 and Ga-Q2 that were drilled further south from well Ga-A1 in the southern Pletmos basin (figure 1.2.1) according to (Roux, 1997) intersected gas saturated sandstones within the synrift succession.

The neighbouring Bredasdorp sub basin (figure 1.21.) has been the focus of most seismic and drilling activity since 1980 (PASA, 2013). As a result several commercial oil and gas fields have been discovered in the Bredasdorp Basin (PASA, 2013).

1.3 Location of the Study Area

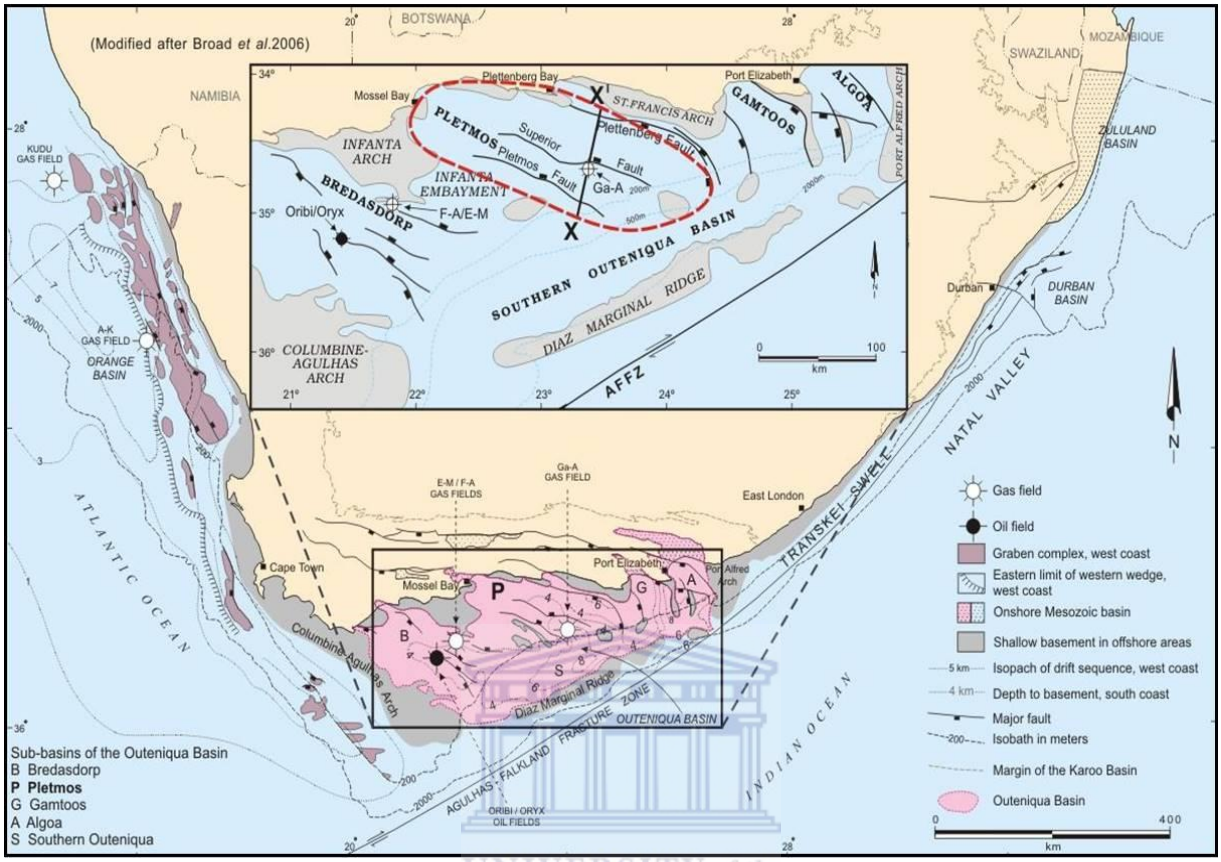

Figure 1.3.1: Location of the Southern Outeniqua Basin, displaying a section of the location of the Pletmos Basin (modified after (Broad, et al., 2006).

The study area of this thesis is located within the southern portion of the Pletmos basin which is one of the sub-basins that forms part of a series of divergent basins located along the southern margin of the African plate where the Indian ocean currents flow as shown in (figure 1.3.1.). Together these sub-basins form the Southern Outeniqua basin.

1.4 Problem Statement and Objectives:

If reservoirs are known to be homogenous their properties would be uniform throughout and the reservoir properties would be easy to predict. However reservoir properties are not uniform.

The purpose of this study is aimed at illustrating the reservoir heterogeneity in the BCII - BCI interval of the GA field, offshore South Africa, with the limited data which is available.

This is achieved by generating a conceptual static model as a predictive tool for the BCII - BCI interval. This encompasses an integration between lithological elements, porosity and permeability distributions which are often further affected by complex fault systems, and the depositional environment. Comparing the results of these elements contributes to the understanding of the stratigraphic, petrophysical and structural framework of the model.

The specific objectives are the following:

- Classify lithofacies from the core studies and interpret depositional environments.
- Characterise the reservoir zones according to the depositional environment.
- Correlate the reservoir sands between the BCII - BCI formation and their distinctive units (well log facies).
- Calibrate the core-measured analysis such as water saturation (Sw), Permeability (K), Porosity (∅) with the calculated parameters of water saturation (Sw), Permeability (K) and Porosity (∅) from the geophysical logs.
- Map out the seismic horizons i.e. 1At1, BCII, BCI and O and the faults to generate a 3D grid, and using a generated linear velocity model for conversion from time to depth.
- Build a lithofacies model based on the upscaled properties of the well logs (lithofacies), and integrate it with the seismic 3D grid.
- Build a permeability and porosity model based on the property modelling of the well logs and integrating it with the seismic 3D grid.

Chapter 2

2.1 Geological Setting

The Outeniqua basin includes offshore rift and post rift basins north of the Algulhas Falkland Fracture Zone (AFFZ) (figure 1.3.1.) and comprises of four synrift sub-basins, namely the Bredasdorp and Pletmos drift basins, which is found in the southern region of the Outeniqua Basin, and the Algoa and Gamtoos which occur the eastern region of the Northern Outeniqua Basin (Brown, et al., 1995). The Outeniqua basin is constrained in the west by the Alguhas – Columbine Arch and in the east by the St Francis Arch (Brown, et al., 1995).

2.2 Paleogeography

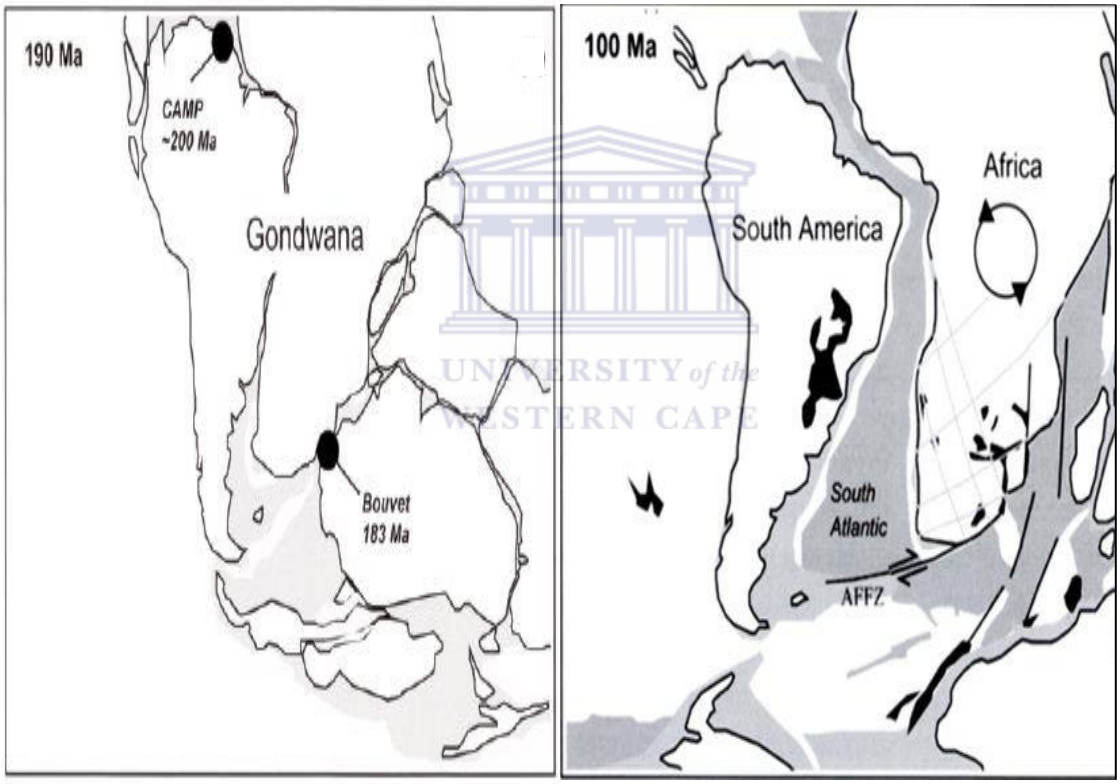

Figure 2.2.1: Schematic diagram showing the breakup of Gondwana 190 - 100Ma after (Scotese, 2002) and (De Wit, et al., 2001).

According to the magnetic survey anomalies of Dingle, et al. (1983), rifting between the African and Antarctic plates was initiated west of Madagascar when Southern Gondwana (figure 2.2.1) began to break up between~143 -142 Ma and 133Ma. South western Gondwana began to diverge at~127 Ma into the African and South America plates along the AFFZ (Larsen & Ladd, 1973) (figure 2.2.1).

The rifting phase in South Africa ended during the Valanginian (figure 2.3.3). This was accompanied by regional uplift and extensive erosion of a drift onset unconformity (126 Ma). During this period the integration of the various Algulhas rift basins (Brown, et al., 1995), occurred which resulted in the initial formation of the of the post rift Pletmos and Bredasdorp Basin. Movement of the Falkland Plateau westward past the Pletmos Basin and Bredasdorp culminated during the early Aptian (~ 112Ma) as a result of a third episode of post rift basement uplift and intense erosion. (Brown, et al., 1995).

2.3 Depositional Setting

The Pletmos Basin covers ~ 18 000km^2 (PASA, 2010) is a filled with Synrift I, Synrift II and post rift Cretaceous sediments locally bounded in the north by the St Francis Arch and in the Southwest by the Infanta Embayment (figure 2.3.1 and figure 2.3.2). The Pletmos basin is sub divided into the Plettenberg, North Eastern, Northern, Southern and South Eastern basin (Brown, et al., 1995) These sub-basins are confined by the Plettenberg, Superior and Pletmos faults.

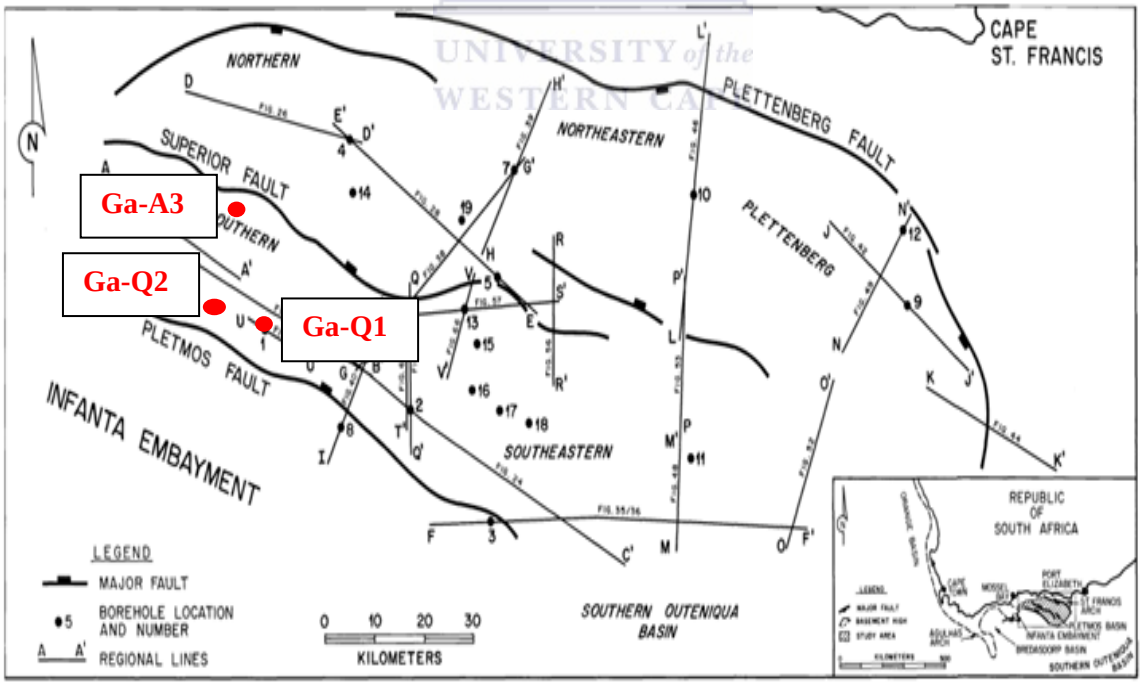

Figure 2.3.1: Map of the Pletmos Basin and its sub basins with its major bounding faults (Brown, et al., 1995).

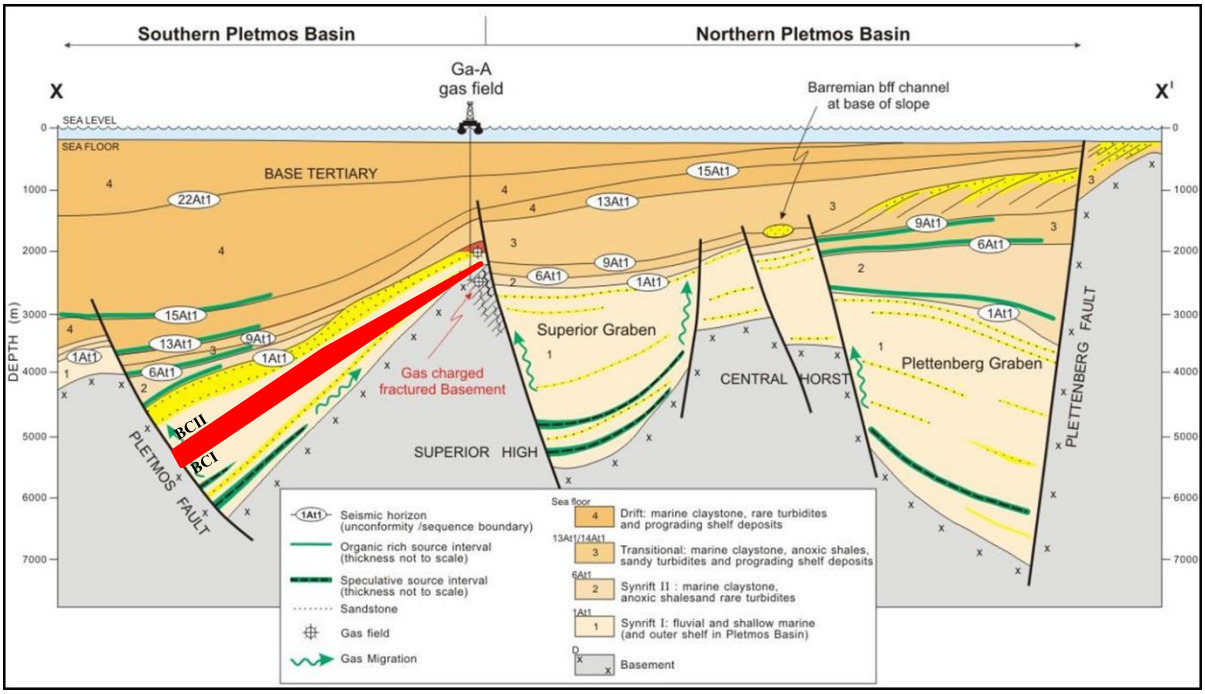

Figure 2.3.2: Schematic geological cross section across the Pletmos sub-basin, illustrating structural styles and stratigraphic subdivision modified after (Roux & Davids, 2010).

The Pletmos Basin throughout its synrift I Cretaceous period was influenced by siliciclastic depositional systems. According to Brown, et al. (1995), changes in the depositional system were as a result of the second order tectonic episodes such as: variations in sediment supply rates, increasing open marine activities, and accommodation and subsidence rates.

Deposition in the basin ranges from restricted fan deltaic systems (126 -117.5 Ma) to river to tide dominated embayment systems (117.5 -112Ma) and to open marine wave and river dominated systems (112-68Ma) (Brown, et al., 1995). In both the Pletmos Basin and Infanta Embayment rift transitional-early drift and late drift phases of sedimentation are recognised with the basin-wide unconformities D, 1Atl and 13Atl delineating the onset of these episodes (figure 2.3.2 and figure 2.3.3). Thick D to 1Atl intervals also occur just to the north of the Superior Fault (figure 2.3.2), as well as in the southernmost Pletmos Basin, north of the Pletmos Fault. D to 1Atl sediments are composed of inner to outer shelf sandstones and claystones with localised non-marine red and green beds. (Mcmillan, et al., 1997).

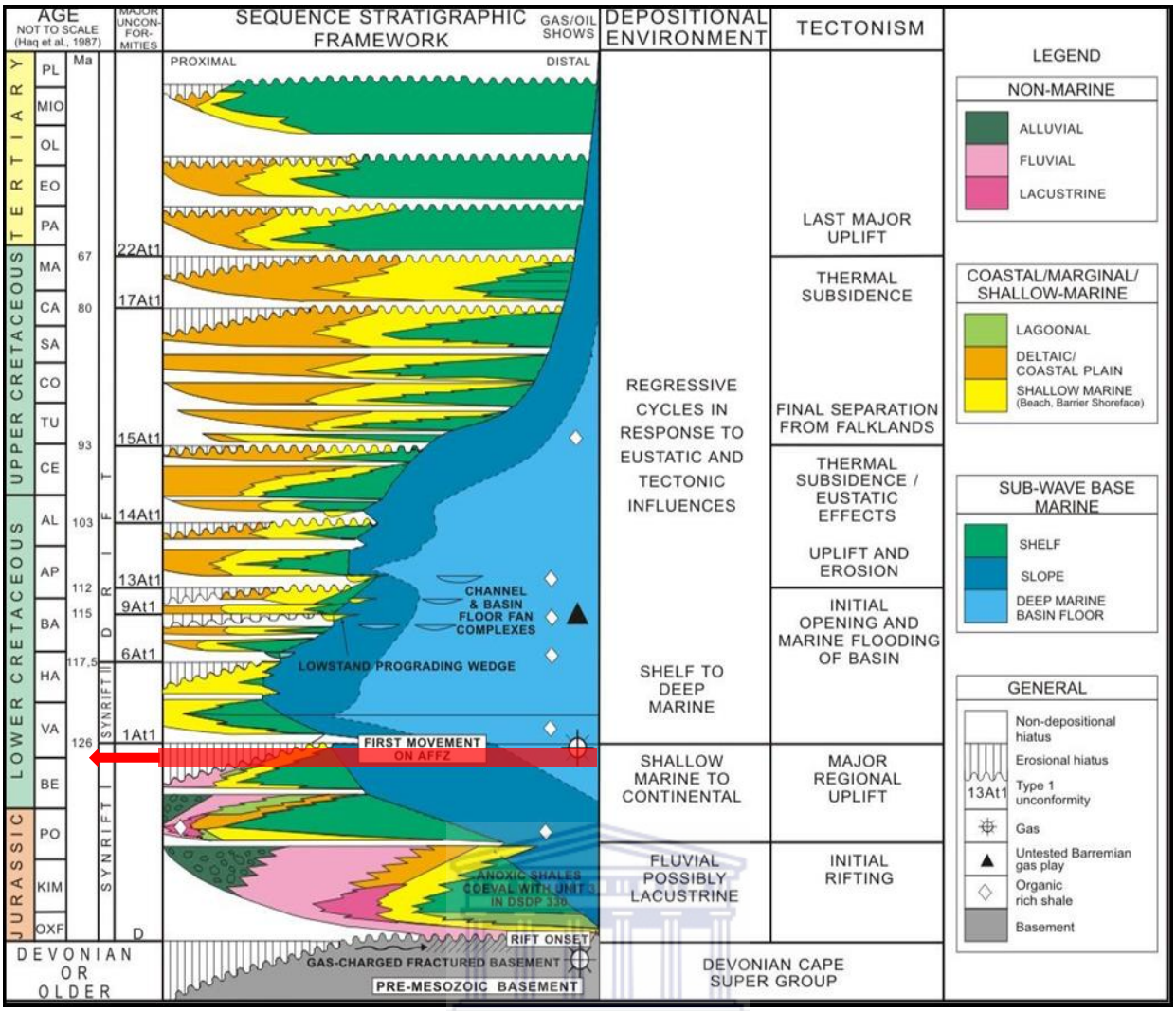

Figure 2.3.3: Generalised stratigraphy of the Pletmos basin and BCII –BCI interval marked in red modified after (PASA, 2010).

The focal area of this study is found between the first phase of rifting (Synrift I), the early Cretaceous sediments and the Devonian Cape Supergroup (figure 2.3.3); referring to (figure 2.3.2) the fill of the late Jurassic grabens comprises of Synrift I sediments and consists of aggradational fluvial sediments in the north and marginal marine in the south of the basin (PASA, 2010). The later Synrift I interval of Lower Cretaceous age sediments consists of fluvial to shallow marine and shelf deposits.

The 1At1 unconformity situated above this later Synrift I interval signifies the initial commencement of the transform movement of the AFFZ and the commencement of the Synrift II which is the second phase of rifting that took place in the Outeniqua basin. The dextral dextral transform movement of the AFFZ caused major subsidence and a deep marine, poorly oxygenated environment prevailed.

2.4 Structural controls on the sediment input.

According to Mcmillan, et al. (1997) from the top of the basement (horizon D) to horizon 1Atl (Kimmeridgian to Late Valanginian) (figure 2.3.3) an extensional stress regime led to horst and graben tectonics, and locally extremely thick accumulations of sediment, most notably in the graben just south of the Plettenberg Fault. Faults such as the Plettenberg, Superior and Pletmos fault impose significant structural control on the basin complex. Limited structural closures for the post rift successions required a focus on the development of stratigraphic trap plays but Upper Jurassic and Lower Cretaceous synrift I sandstone reservoirs have structural closures (Brown, et al., 1995).

2.5 Basement control

The pre-Mesozoic basement has been penetrated by a few wells in the Pletmos Basin, but on basement highs only, consists mainly of the Ordovician-Silurian Table Mountain group quartzites belonging to the Palaeozoic Cape Supergroup (Mcmillan, et al., 1997).

2.6 Stratigraphic controls

Stratigraphic controls in the area are influenced by the deposition of the lowstand stand reservoirs: seals are composed of marine transgressive shale, marine condensed sections (Brown, et al., 1995). Potential limiting factors within the lowstand tracts are unfavourable diagenetic damage to the porosity and permeability, textural, and grain constraints which lead to poor migration of the hydrocarbons. (Brown, et al., 1995).

2.6.1.1 Facies

According to McMillan, (2003), the stratigraphic succession found within the Pletmos Basin is very similar to the depositional sequence in the Bredasdorp. The Kimmeridgian to Late Valanginian (horizon D to 1At1) graben fill succession (McMillan, 2003), comprises of a marine shelf (figure 2.3.3), grey claystones and glauconitic sandstones with locally red fluvial claystones present and in the proximal setting, occasional conglomerates.

Chapter 3:

3. Research Methods

The composition of the data set is shown in the table below. Sedimentary facies logs were created by using Sedlog. Structural interpretation such as fault and horizon mapping, velocity modelling, upscaling and petrophysical modelling was done on software developed by Schlumberger: Petrel 2013. The petrophysical analysis of the well logs was done using Interactive Petrophysics.

Data set:
• Four 2D Seismic lines
• Three Wells (Ga-A3, Ga-Q1, Ga-Q2)
• Completion reports (Ga-Q1 and Ga-Q2 only)
• Core Data (Ga-A3 and Ga-Q1)
• Geophysical log suites (GR, DT, RHOB, NPHI, ILD, MSLU, SFLU).
Software:
• Petrel 2013(Schlumberger)
• Interactive Petrophysics V4.2 (Synergy)
• Sedlog v3.0

Table 3. Data set of this study.

Workflow undertaken for this study:

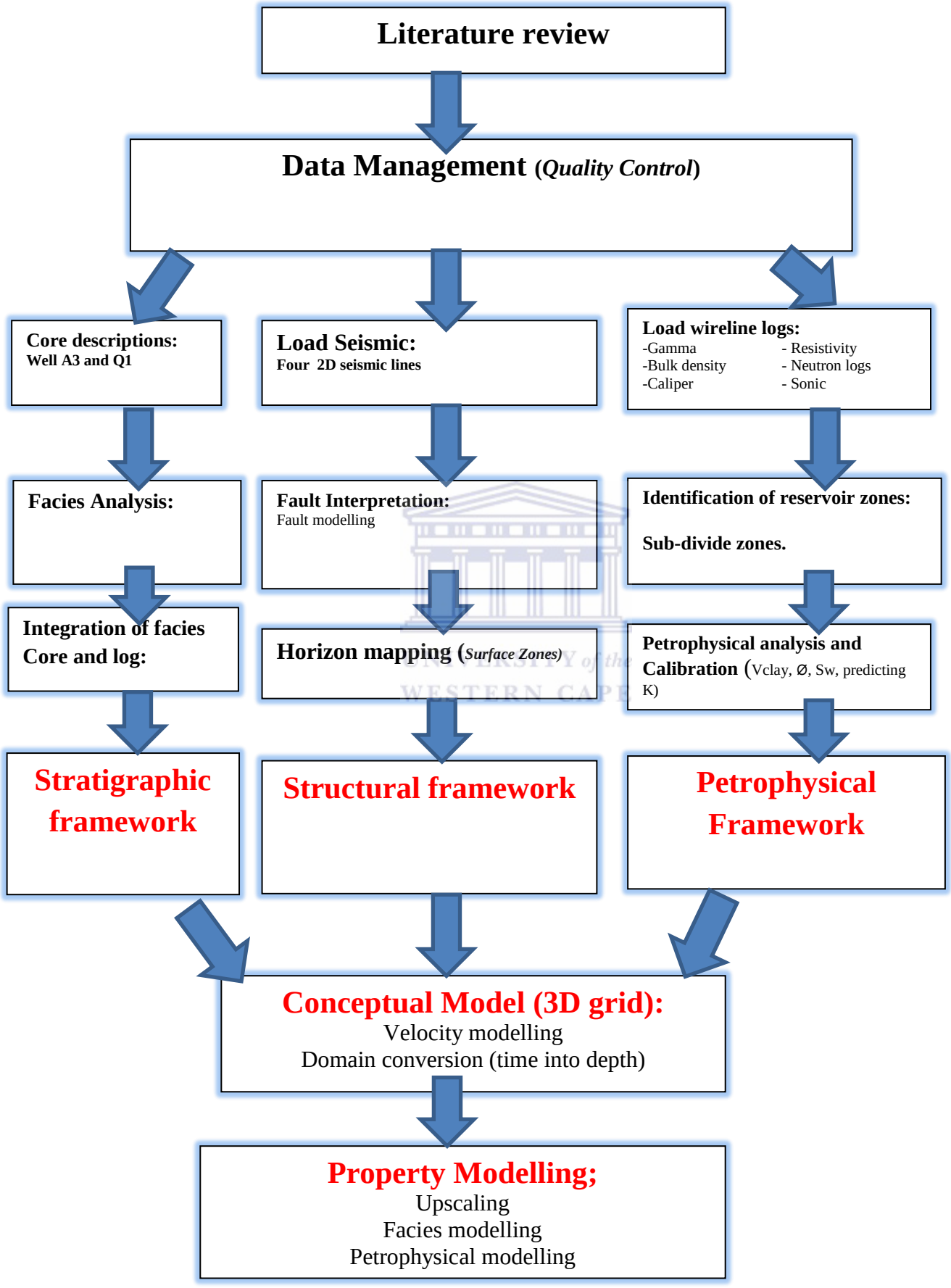

3.1 Stratigraphic concepts

3.1.1 Coring

In order to describe the reservoir properties, it is important that the reservoir core is retrieved in order to analyse the reservoirs properties - grain sizes, porosity and permeability - from the reservoir interval of interest which is integrated with the geophysical logs. According to Blackbourn (1990), during drilling and just before logging the wellbore, samples are of continuous core which is retrieved via a core barrel. This is a direct physical sample of the formation (Blackbourn, 1990).

3.1.2 Facies

Facies analysis assists in building a facies model which describes a specific depositional environment in a short summary. Based on the combination of lithology, texture and internal sedimentary structures can be assigned to each facies identified.

3.1.3 Wireline Logs

The logs were made available in LAS format for each of the wells. Petrel and Interactive Petrophysics software was used to view the log files to identify facies successions as well as generate the petrophysical parameters.

3.1.4 Gamma log shapes

The relationship between the gamma ray log and the grain size is represented by shape of the gamma ray response (Rider, 1996). The shapes on the gamma ray log displays trends indicated by the (figure 3.1.4) cylindrical, bell, symmetrical and serrated motifs which can be interpreted as grain size trends and be associated with facies successions.

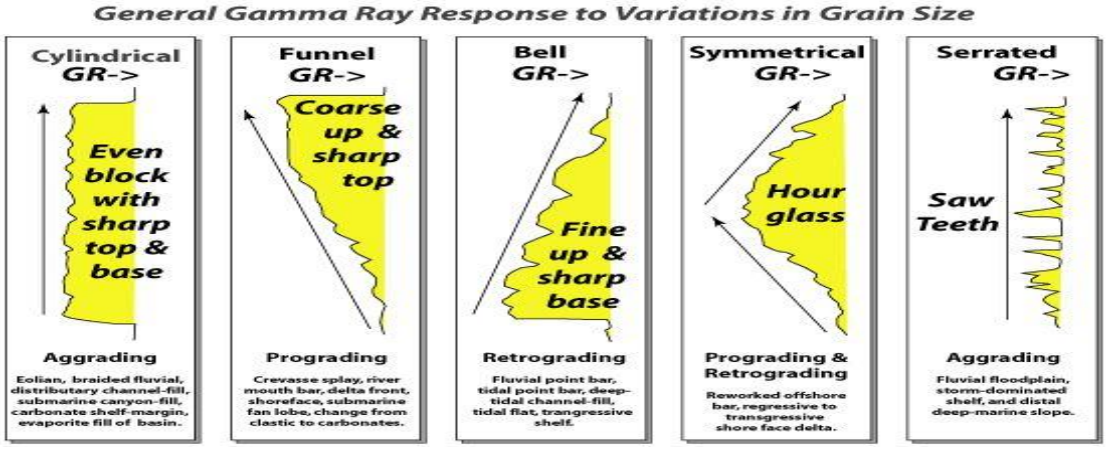

Figure 3.1.4: Direct correlation between facies and logs shapes (SEPM. & Geololgy., 2013).

3.2 Petrophysical parameters

Petrophysics is the study used to evaluate the properties of the rock. Petrophysical parameters are obtained from core analysis which is carried out in the laboratory and calibrated with the measurements made from the geophysical logs.

3.2.1 Porosity

Porosity is expressed as the percentage of pore volume or void space, or that volume within rock that can contain fluids.

$$Porosity\ (\emptyset) = \frac{Volume\ of\ void\ space}{Total\ volume\ of\ the\ rock}$$

Porosity comprises of primary porosity which refers to the pore space which is available at the time of deposition. Secondary porosity is the porosity that's available after deposition which results from factors like dissolution of cements, fracturing and recrystallization of minerals. Therefore, effective porosity is the porosity of the pores which are connected and available for free fluids.

Effective porosity is calculated based on the formation bulk density (p_b) as a function of matrix density (p_{ma}), porosity and formation fluid density (p_f)

Density porosity if defined as:

$$\emptyset den = \frac{Pma - Pb}{Pma - Pf}$$

3.2.2 Porosity logs

In this study the core data was calibrated to effective porosity rather than total porosity due to the Vclay correction which was taken into consideration. The PhiDen log and the core calibrated very well.

3.2.3 Permeability

Henri Darcy conducted experiments in 1856 to classify the concept of permeability. Permeability is a measure of ease with which fluids flow through a formation. Permeability is mostly affected by grain size, pore throat sizes and continuity of the pore network, clay minerals and fractures. Therefore permeability is related to the connectivity of the pores and fractures with a given formation or rock. Permeability for oil, water and gas flow is a dynamic parameter therefore in the lab absolute, static permeability is measured.

Permeability is expressed in the following equation (Glover, 2000) as:

$$Q = \frac{k\mathrm{A}(\mathrm{Pi} - \mathrm{Po})}{\mu\, L}$$

Where:

	Q	=	Flow rate (cm^3/s or m3)
	P_o	=	Outlet fluid pressure (dynes/cm^2 or Pa)
	P_i	=	Inlet fluid pressure (dynes/cm^2 or Pa)
	μ	=	Dynamic viscosity of fluid (poise or Pa.s)
	L	=	Length of the tube (cm or m)
	k	=	Permeability of the sample (darcy or m^2)
	A	=	Area of the sample (cm^2 or m^2)

The unit in which permeability is measured is known as the darcy, but more commonly a milidarcy (mD) is used, which is a thousandth of a darcy. Permeability is measured vertically (Kv) and Horizontally (Kh). Klinkenberg permeability is commonly used in the oil and gas industry for the correction for gas flow. Cross plots of permeability can be classified as in (figure 3.2.3 and table 3.2.3 1).

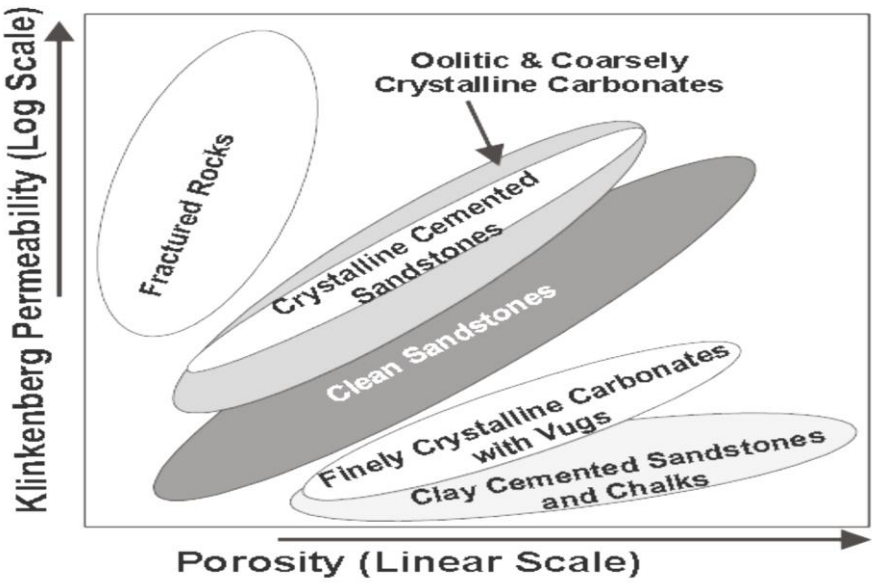

Figure 3.2.3: Porosity versus permeability plot (Glover, 2000).

Classification	Permeability (mD)
Fair	1-10 md
Good	10 – 100 md
Very Good	100 – 1000 md

Table 3.2.3-1: Permeability classification (Glover, 2000).

Predicted log permeability was calculated by using a linear regression, from using the permeability estimated from the regression analysis of the core porosity versus permeability plot. According to SPE (2013) when a straight-line relationship between log(K) and ∅ exists the computation of a predictor for log(K) is direct. By adopting a polynomial in ∅ curvature in the log (K) is accounted for.

Using the following equation whereby:

$$Log(k) = a + b\emptyset$$

Well	Porosity-Permeability function	Correlation Coefficient (R^2)
Ga-A3	(K) = 10^(-0.216072 + 1.560651* Ø)	0.351704
Ga-Q1	(K) = 10^(-1.89047 + 939305* Ø)	0.513834

Table 3.2.3-2: Porosity – Permeability functions for well Ga-A3 and Ga-Q1.

3.2.4 Vclay/Vshale

The Vclay/Vshale analysis was done using the Interactive Petrophysics software for the evaluation of clay in the sandstone reservoirs. It was calculated based on the linear method using the natural gamma ray log using the Vclay/Vshale steiber equation to calculate Vclay.

Gamma Ray Index

$$I(GR) = \frac{Gr(\log) \ - \ Gr\ (min)}{Gr\ (max) - Gr\ (min)}$$

Where:

I_{GR} = gamma ray index

GRlog = Gamma ray reading from the log

GRmin = minimum GR

GRmax = maximum GR

Vshale = I_{GR} Linear response

Vshale = $0.08(2^{3.7*IGR})$, Larionov (1969), Tertiary rocks

Vshale = $IGR/(3 - 2xIGR)$, Steiber (1970)

Vshale = $1.7-[3.38 - (I_{GR}- 0.7)^2]^{½}$, Clavier (1971)

Vshale = $0.33 \times (2^{2*IGR} - 1)$, Larionov (1969), Older rocks

3.2.5 Temperature gradient:

An geothermal gradient of 3.85º c/100m was used to calculate the temperature curve. The geothermal gradient was obtained from the well completion report.

3.2.6 Fluid saturation

Fluid saturations are determined from the core analysis (Crain, 2001). Fluid saturation is the fraction or percentage of pore space which is occupied by a certain fluid.

Expressed by the following equation as:

$$Fluid\ saturation(Sf) = \frac{Formation\ fluid\ occupying\ pores}{Total\ pore\ space\ in\ Rock}$$

3.2.7 Determining Water Saturation (Sw)

Water saturation is the ratio of water volume to pore volume (Crain, 2001). Water saturation is calculated based on effective porosity and the resistivity log (Crain, 2001). There are various equations used in determining the water saturation of a formation, such as the Archie (1942) formula.

Whereby Sw of the reservoir's uninvaded zone is calculated by:

$$Sw = \left(\frac{a \text{ x } Rw}{\emptyset^m Rt}\right) 1/2$$

Where:

Sw = water saturation of the uninvaded zone (Archie method)

Rw = resistivity of formation water at formation temperature

Rt = true resistivity of formation

Ø = porosity

a = tortuosity factor

m = cementation exponent

n = saturation exponent which varies from 1.8 to 2.5 but is normally equal to 2.0

Water saturation is calculated from the resistivity log and can be used for relating Sw to resistivity and porosity, where as the most common formula for SW is the Archie formula but it is only applicable to formation with clean sandstones. The most applicable formula was the Indonesia formula.

3.3 Geometrical Concepts

3.3.1 Velocity Model

A velocity model is applied when converting from time to depth.

Constant velocity is: V = Vint

K = (vertical velocity gradient)

Z = travel time

Liner velocity (Linvel): $V = V0 + kZ$ ……1

After calculation: Z=ZT+V0 (t-Tt)……..2

This is to say at each point in the model, an interval the velocity at that point is V0+kZ. The following figure 3.3.1 illustrates a cross section of a 3D grid (Schlumberger, 2013).

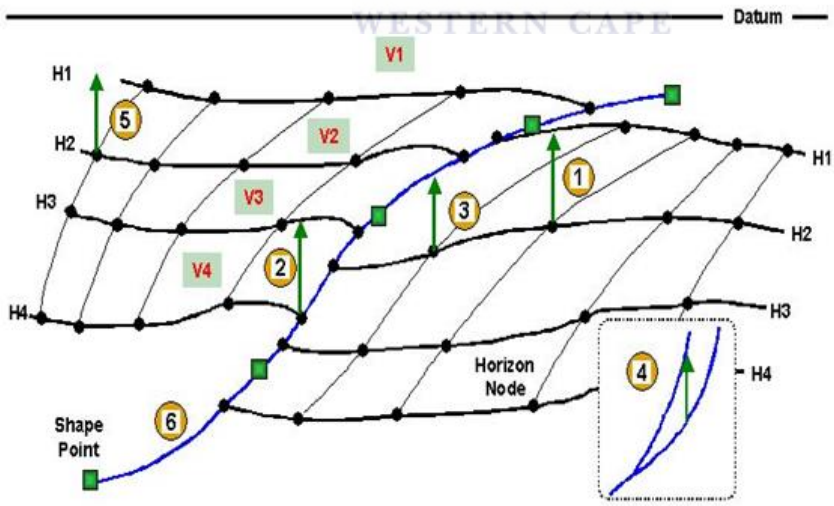

Figure 3.3.1: Shows the different nodes of the horizons being depth converted using the linear velocity algorithm (Schlumberger, 2013**)**.

3.3.2 Upscaling

Upscaling is the concept whereby grid cells through which the wells pass, are assigned values derived from the log. For each cell an averaged is calculated according to the specified algorithm to produce one log value for that cell. The upscaled value will then correspond to the value that is most represented in the log for that particular cell (Schlumberger, 2013).

Figure 3.3.2 Upscaled well logs that will be used for property modelling in the 3D grid (Schlumberger, 2013).

The primary objective of geological characterisation is to enable the prediction of spatial variation in the geological model away from the well bores. The well is the only locality where the data from the well is honoured and all the data away from the well is extrapolated. A geological model helps to constrain the geostatisical modelling by setting trends in the facies, thickness and orientation. In the geostatisical modelling deterministic or stochastic algorithms are used for the facies and petrophysical modelling.

A deterministic model when simulated will give similar results as to the input data. When using a few data points to simulate the uncertainty in the deterministic model, the deterministic model will not display the uncertainty as much as compared to the stochastic model where as when applying the stochastic algorithm the model uses a random seed in addition to the input data (figure 3.3.3). The result of the model will have a distribution trend that's more typical of real case scenarios (Schlumberger, 2013).

The stochastic algorithm that was applied was the sequential Gaussian algorithm. This algorithm distributes continuous petrophysical properties such as porosity and permeability into the 3D model. A gaussian simulation produces a realisation of the property which honours the well data and also honours the histogram for the property which is derived from the well data.

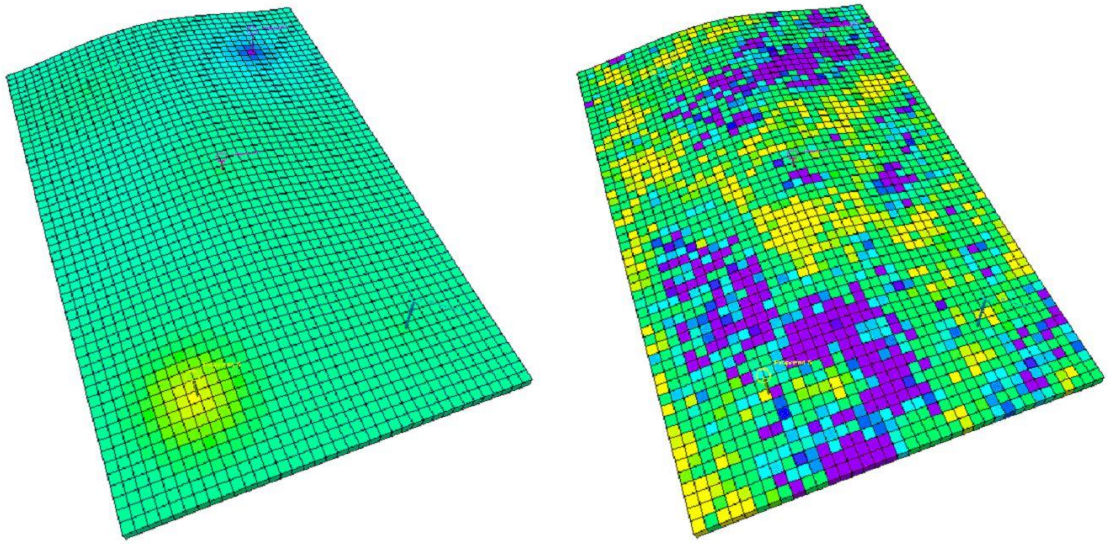

Figure 3.3.3: An example of deterministic modelling (Kringing algorithm) on the left and Stochastic Model (Sequential Gaussian) on the right. (Schlumberger, 2013).

Chapter 4:

4. Results

4.1 Introduction:

This chapter is divided into four sections, namely: stratigraphic framework, structural framework, petrophysical analysis and the geometrical modelling. The basis of the results are based on four 2D seismic lines and three wells as shown below in figure 4.1.1 which are located within the southern region of the Pletmos basin. The principal target zones were the shallow marine sandstone units (BII - BI). This interval of sandstone is the main gas bearing zone in the wells Ga- A3 and Ga-Q1 and it was assumed that this could be the same for well Ga-Q2.

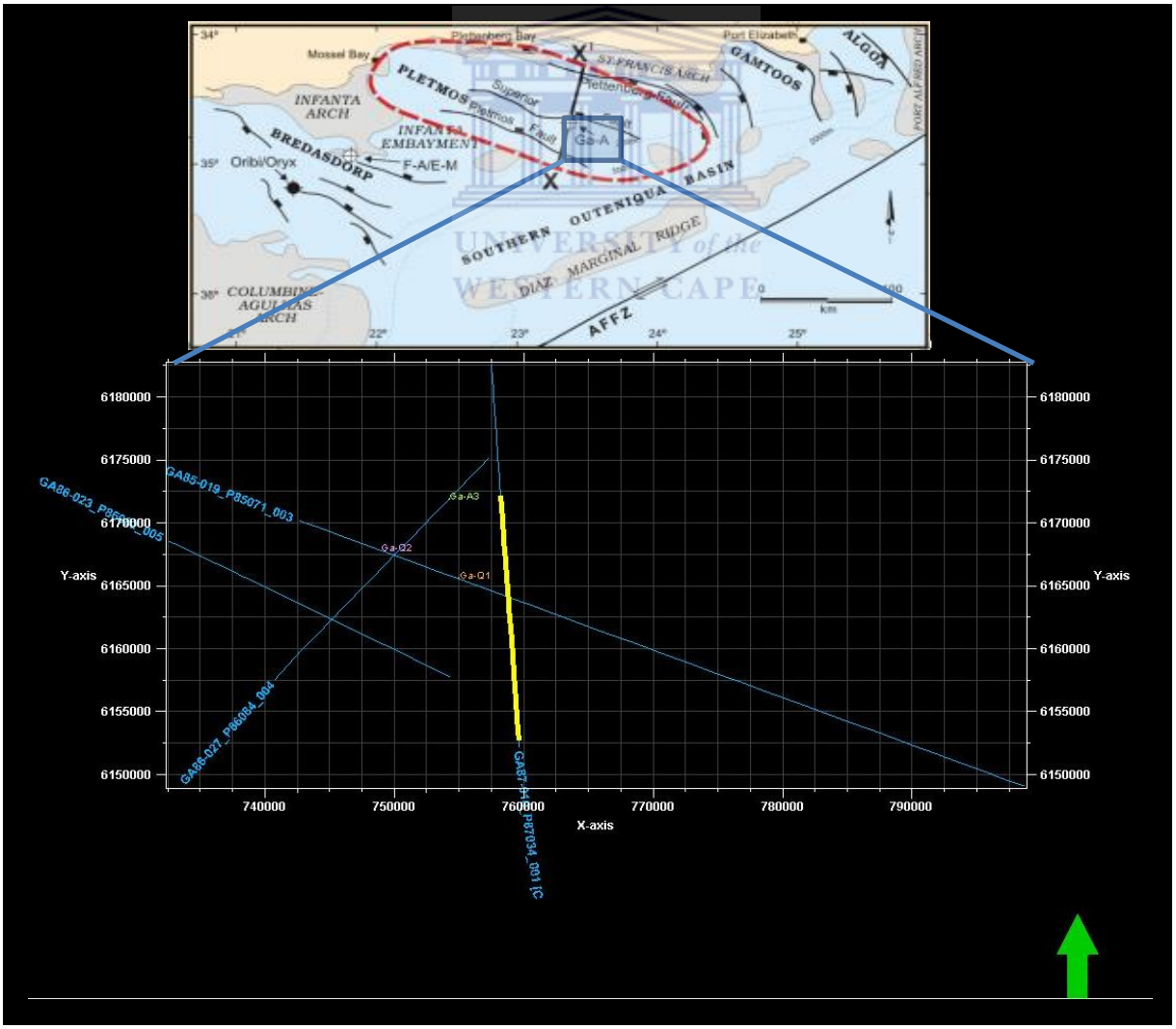

Figure 4.1.1: Study area: base map of the Pletmos basin on a 2D map. Insert modified after (Broad, et al., 2006).

4.2 Stratigraphic Frame work

4.2.1 Introduction

The purpose of this section is to introduce a stratigraphic framework for the study area. A stratigraphic framework assists in a more accurate interpretation of the depositional environment and the lithofacies geometries of unknown portions of the basin or study area (SEPM. & Geololgy., 2013).

The approach taken was to analyse and integrate the data from the cores, wireline logs (GR log), lithofacies reports and well completion reports. From the cores, facies are recognised and from the facies the associated depositional system is defined to form a sedimentary model, the wells are correlated according to the respective reservoir zones and were sub divided into sub zones A and B across wells Ga-A3, Ga-Q1 , Ga-Q2 as seen in the correlation panel (figure 4.2.1).

The principal target reservoirs of this study are the reservoir zones that were targeted below the 1At1 unconformity found between the interval BII to BI. They were prognosed to be composed of stacked sandstone units which were mainly associated with coarsening upward sequences.

Well Ga-A3 and Ga-Q1 are located within the transition zone; where the shallow nertitic sandstone has been deposited on the shoreface. In well Ga-Q2 the BII to BI interval comprises of sandstone units which are related to beach deposits.

The reservoir zones between BII - BI were sub divided into two major zones, A and B for correlation purposes. These two zones are separated by a claystone and siltstone package (indicated by the red arrows on figure 4.2.1). In well Ga-A3 this claystone siltstone package is 20m thick and in well Ga-Q1 150m thick and thins out towards well Ga-Q2. The sandstone packages tend to increase in thickness from well Ga-A3 towards Ga-Q2.

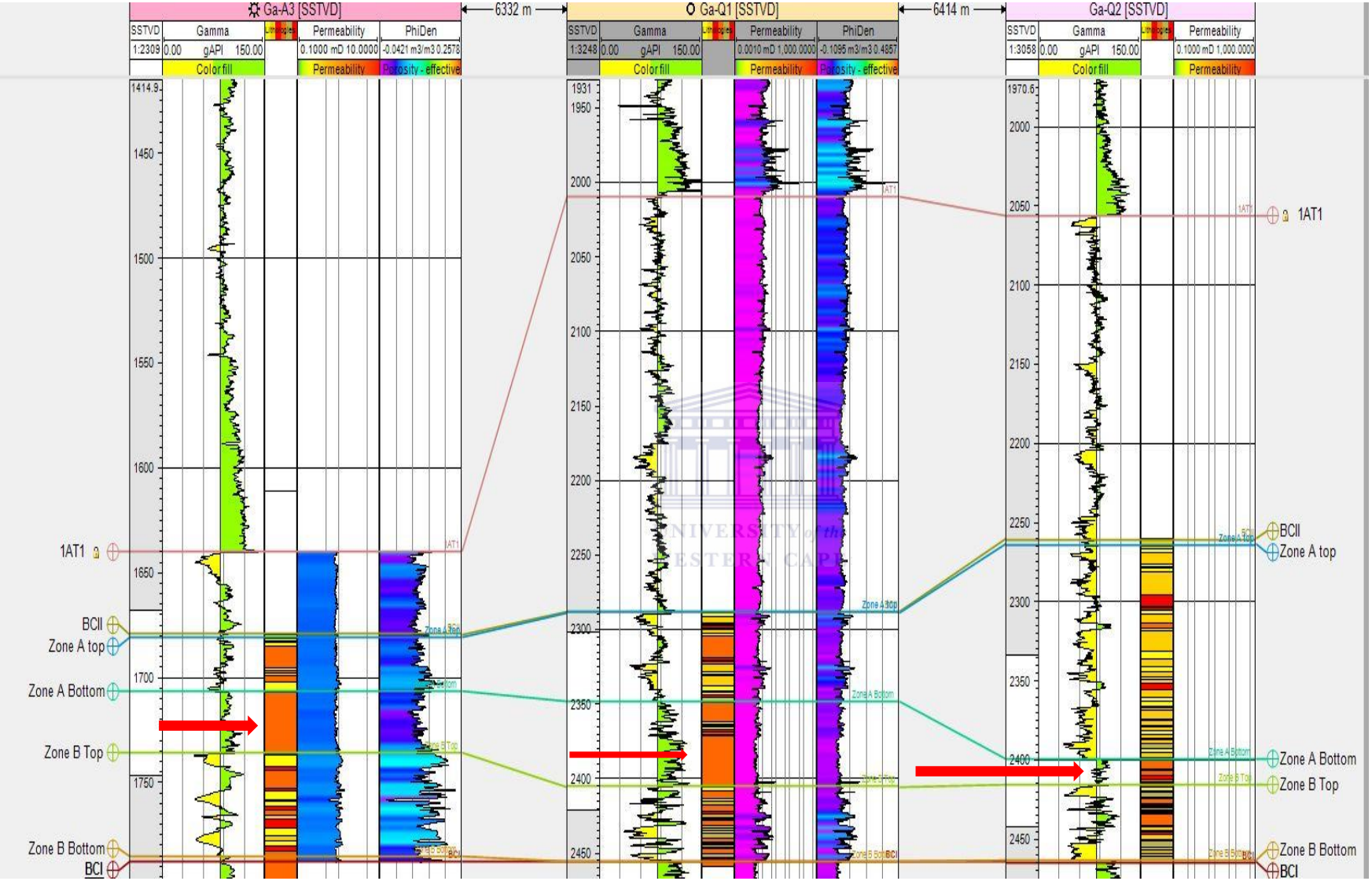

Figure 4.2.1: Stratigraphic correlation of the study area: the BC II - BCI interval and the sub divided reservoir zones A and B correlated from wells Ga-A3, Ga-Q1 and Ga-Q2.

4.2.2 Facies Analysis

Core data and core descriptions were examined for wells Ga-A3 and Ga-Q1 to characterise and interpret the facies. No core data was available for well Ga-Q2. Four main lithofacies were identified and are shown in table 4.2.2-1.

Facies Classification

Class (Facies association)	Lithofacies code	Lithology	Physical Sedimentary Structures	Interpretation
A	A1	Lithic Fg sandstones	Small scaled sized 3mm pebbles, Mud intraclast.	Sub tidal (Thin channel lag)
	A2	VFg sandstone	Sandstone intercalated with 1 -2mm clay lenticles	Sub tidal
	A3	Heterolithic Fg sandstone	Planar lamination with cross bedding.	Sub tidal
	A4	Fg – Cg sandstone	Sandstone with calcite cement in abundance	Sub tidal (channel)
B	B1	Heterolithic Vfg to Fg sandstone	Ripple lamination, Bioturbation Clay drapes.	Intertidal to intertidal Flat
	B2	Fg sandstone	Flaser bedding , mud drapes, Bioturbation.	Intertidal Flat
	B3	Fg to Mg sandstone	Trough cross bedding, planar lamination.	(Sub tidal) Tidal bar or barrier
C	C(5)	Siltstone and claystone	**N/A**	**Background**
D	D (5)	claystone	**N/A**	**Background**

Note: Vfg= very fine grained, Fg= fine grained, Mg=Medium grained

Table 4.2.2-1: Lithofacies descriptions of the reservoir sandstones of BCII to BCI.

The lithofacies of interval BCII – BCI were subdivide into facies A (Table 4.2.2 1) and further subdivided into sub lithofacies A1 to A4 which the facies A has been interpreted to be sub-tidal. Facies B (table 4.2.2-1) has been sub divided into sub lithofacies B1 to B3 based on the sedimentary structures bioturbation intensity and grain sizes. Lithofacies B has been interpreted as mid intertidal. Siltstone and claystone were placed into facies association C and D respectively.

Sub tidal (Lithofacies A1, A2 and A3) (figure 4.2.2.)

Facies A1: Comprises of a light grey to light greenish moderately sorted fine grained glauconitic sandstone grains that are slightly angular to moderately rounded, with small scaled 3mm pebbles found at a depth of 1773m. Core photo of facies A1 with the greyish sandstone with mud drapes and clay stone intraclast which could be the base of a channel.

Facies A2: Very fine grained sandstone streaks (dm) occasionally intercalated with 1- 2 mm clay lenticles. Sandstone grains are moderately sorted, grain shape is slightly angular to rounded. Note that the mm-cm clay lenticles are altered by bioturbation and some fluid escape. The clay lenticles could indicate fluctuating and alternating currents of low energy.

Facies A3: Fine grained sandstone angular to well rounded, grey with planar lamination and cross bedding. Centimetre scale low angle crossbeds to ripple crossbeds a sign of weak traction currents.

Facies A4: Localised intertidal channel with fine sandstone with cm-mm pebble fragments (Figure 4.2.2.).

Tidally influenced (Lithofacies B1, B2 and B3) (figure 4.2.2)

Facies B1: Composed of angular to rounded, very fine to fine grained light grey glauconitic sandstone, rippled and trough bedding has be reworked through moderate to intense bioturbation. The sediments are slightly glauconitic with vertical burrows or horizontal burrows, the claystone laminae is broken up due to the bioturbation conjugate fracture sets are present. **Facies B2:** Composed of greyish very fined grained, angular to rounded sandstone with flaser bedding and mud laminae is trapped within the trough of the ripple

Facies B3: Light greyish planar lamination sandstone which is infilled with coarser sand is p characterised by the trough cross bedding which is infilled with coarser sand and capped by clay drapes.

Figure 4.2.2: Lithofacies A core interval at a depth interval of 1772m to 1778m and lithofacies B at a depth interval of 2329m to 2346m of BCII and BCI interval.

4.2.3 Log responses

The contact of the second order 1At1 unconformity between wells Ga-A3, Ga- Q1 and Ga-Q2 is situated just above BCII. This boundary is recognised by a noticeable increase in gamma ray response. Each well and its associated zones of interest are discussed following in the sequence from well Ga-A3 to well Ga-Q1 and well Ga-Q2.

4.2.3.1 Well-Ga-A3

One core was cut in the interval horizon BII to BI, another core was cut just below the 1AT1 sequence boundary but doesn't fall within the primary zones of interest. The core depth range for BII to BI is located at 1769.08m to 1779.75m with effectively 10m that has been cored, but only 5m of core was available. The gamma ray response indicated a sequence of coarsening upward and fining upward trend zones that were investigated as indicated in figure 4.2.3. The gamma ray log response for well Ga-A3 is interpreted as a fining upward sequence in zone A and towards the lower section in zone B just above the BCI, a series of fining and coarsening upward sequences is shown with abrupt tops in between these. The dominant features are listed in table 4.2.3-1 below.

Zone	Core depth (m)	Typical facies	Log pattern	Depositional Environment	Gamma ray (API Units)
Ga- A3 Zone A	No core		Bell shaped (Change from sand to shale)	Shoreface	80 - 120
Ga- A3 Zone B	1772 to 1778	B1, B2, B3 C1	Hour glass	Barrier bar	50 - 75

Table 4.2.3-1: Associated log (GR) patterns with cored zones.

4.2.3.2 Well Ga-Q1

The interval from the 1AT1 unconformity to horizon BI is representative of a large transgressive phase as defined by the gamma log. In zone A (figure 4.2.3) the gamma ray log displays a funnel shape indicative of two individual sequences of coarsening upward trends with abrupt tops. Zone B displaying a shallowing upward/dirtying up of alternating sandstone and clay units, this trend indicates a possible decrease in depositional energy as shown in table 4.2.3-2,the depositional environment becomes more tidal.

Zone	Core depth (m)	Typical facies	Log pattern	Depositional environment	Gamma ray (API Units)
Ga- Q1 Zone A	2329 - 2346	B4, B5, B6	Funnel	Tidal flats to Intertidal.	50 - 90
Ga- Q1 Zone B	No core		Serrated	Possible bars	50 – 75

Table 4.2.3-2: Associated log (GR) patterns with cored zones Ga-Q1.

4.2.3.3 Well Ga-Q2

Reservoir sandstones (figure 4.2.3) are slightly thicker than Ga-Q1, due to the fact that the well is situated in a more proximal position relative to the sandstone source. This is quite evident in the dominant gamma ray log response of BCII and BCI which shows the three serrated units separated by three minor transgressive phases (table 4.2.3-3).

Zone	Core depth (m)	Typical facies	Log pattern	Depositional environment	Gamma ray (API Units)
Ga- Q2 Zone A	No core		Serrated	Proximal marine slope	80 – 120
Ga- Q2 Zone B	No core		Serrated	Proximal Marine slope	50 – 75

Table 4.2.3-3: Associated Log (GR) patterns with cored zones Ga-Q2.

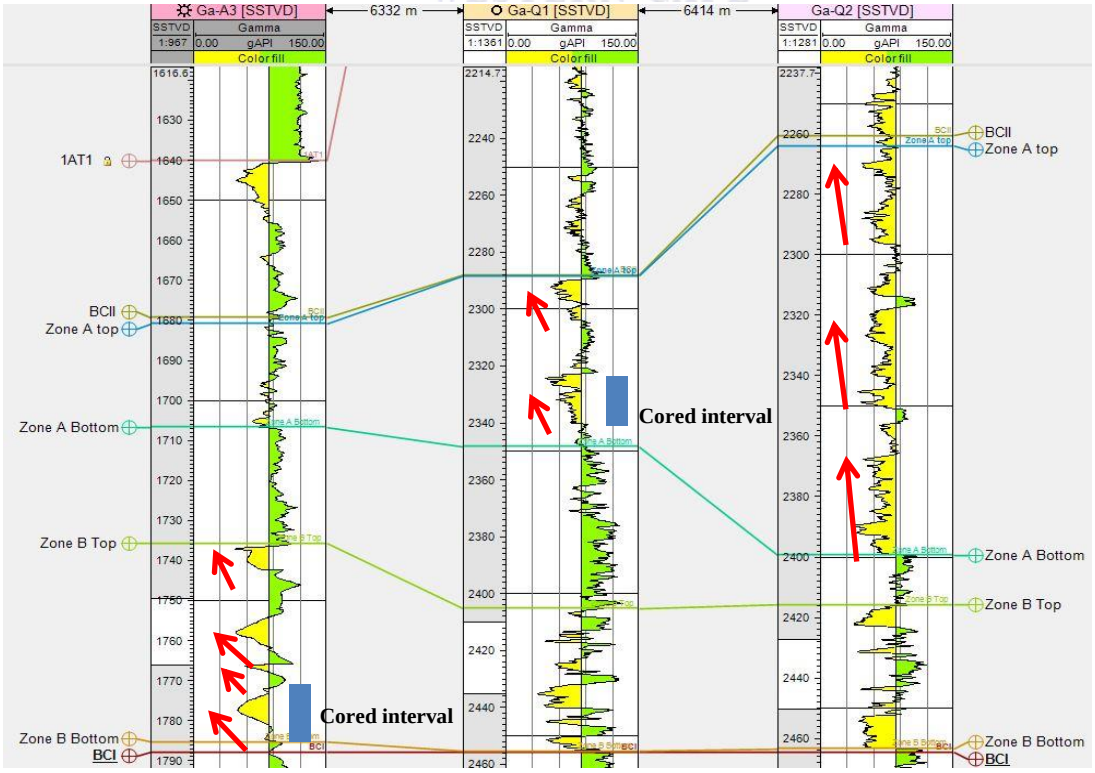

Figure 4.2.3: Identification of log shapes based on the geophysical log properties.

4.3 Structural Framework

4.3.1 Introduction.

Stratigraphic study is always preceded by structural interpretation (Neal, et al., 1993). A structural analysis of the fault and horizon interpretation was done. The mapping of the horizons of the synrift I unit were mapped out across the four seismics, the horizons are namely the 1At1, BII, BI and O as shown below in figure 4.3.1. The red arrows marks the top and base of the interval of interest found between the BCII-BCI. Line Ga85-019 illustrates the general characteristics of the seismic data. This (Figure 4.3.1) line passes through the middle of the study area as defined by the base map (Figure 4.1.1).

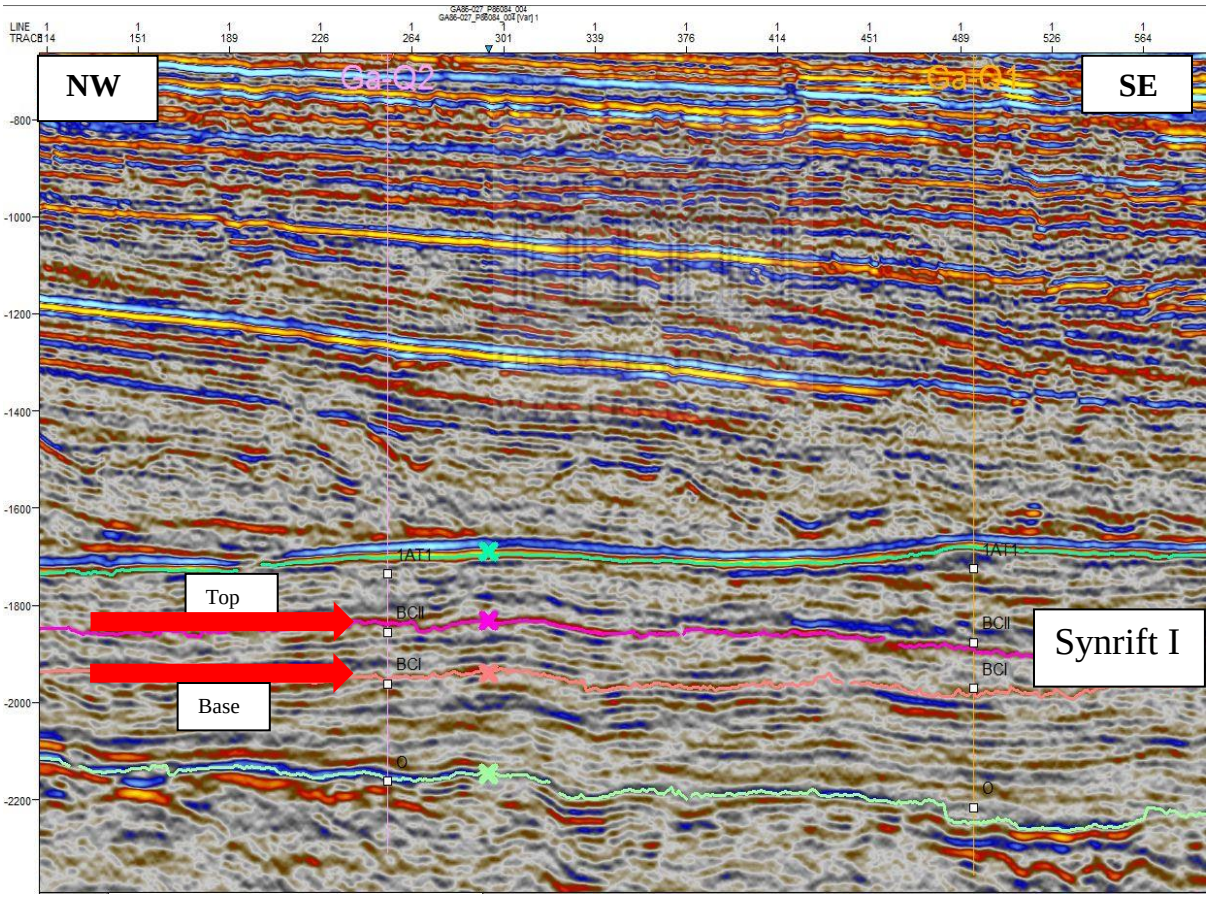

Figure 4.3.1: Line Ga85-019 seismic section, horizons BCII - BCI interval interpreted with well Ga-Q2 and Ga-Q1 intersecting the BCII –BCI interval.

BCII - BI interval forms part of the shallow marine sequence and sits below the erosional 1At1 unconformity (figure 4.3.1). Well Ga-Q2 lies 6.5km northwest of the Well Ga-Q1. The BCII to BCI interval is influenced by a very complex fault system which comprises of minor local faults and major faults.

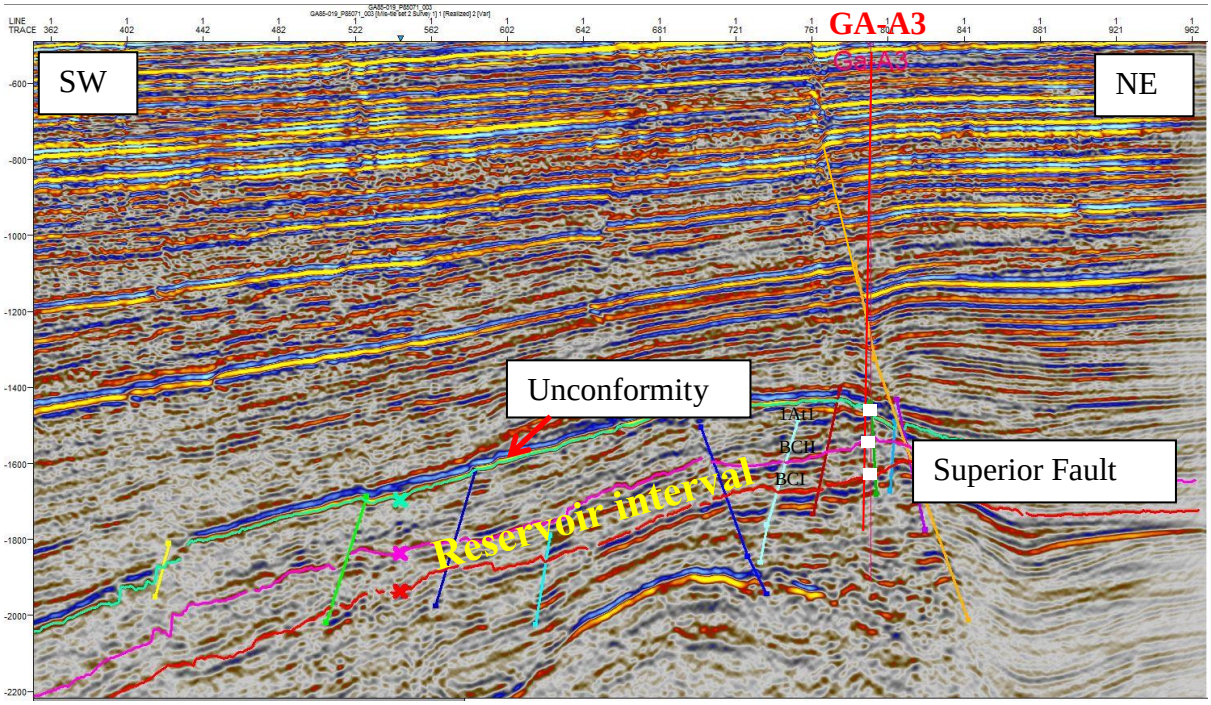

Figure 4.3.2: Line Ga86-027 showing the interpretation of the BCII and BCI interval with Well Ga-A3 passing through the major Superior fault in the Pletmos basin.

Well Ga-A3 (figure 4.3.2), intersects the major Superior fault just above the 1At1 unconformity. The second order erosional unconformity 1At1 (figure 4.3.2) that is found throughout the basin is one of the sequence boundaries that occurred due to the dominant tectonic control on the sedimentation in the basin. The minor antithetic faults shows (figure 4.3.2.) West North West to East South East strike fault. The major Superior fault shows a North West to South East strike. These faults formed as a result of the dextral transtensional stress which was exerted in the north of the basin.

The key reservoir intervals fall within the BCII-BCI interval indicted on the seismic line (figure 4.3.2.) are intersected by the minor normal faults.

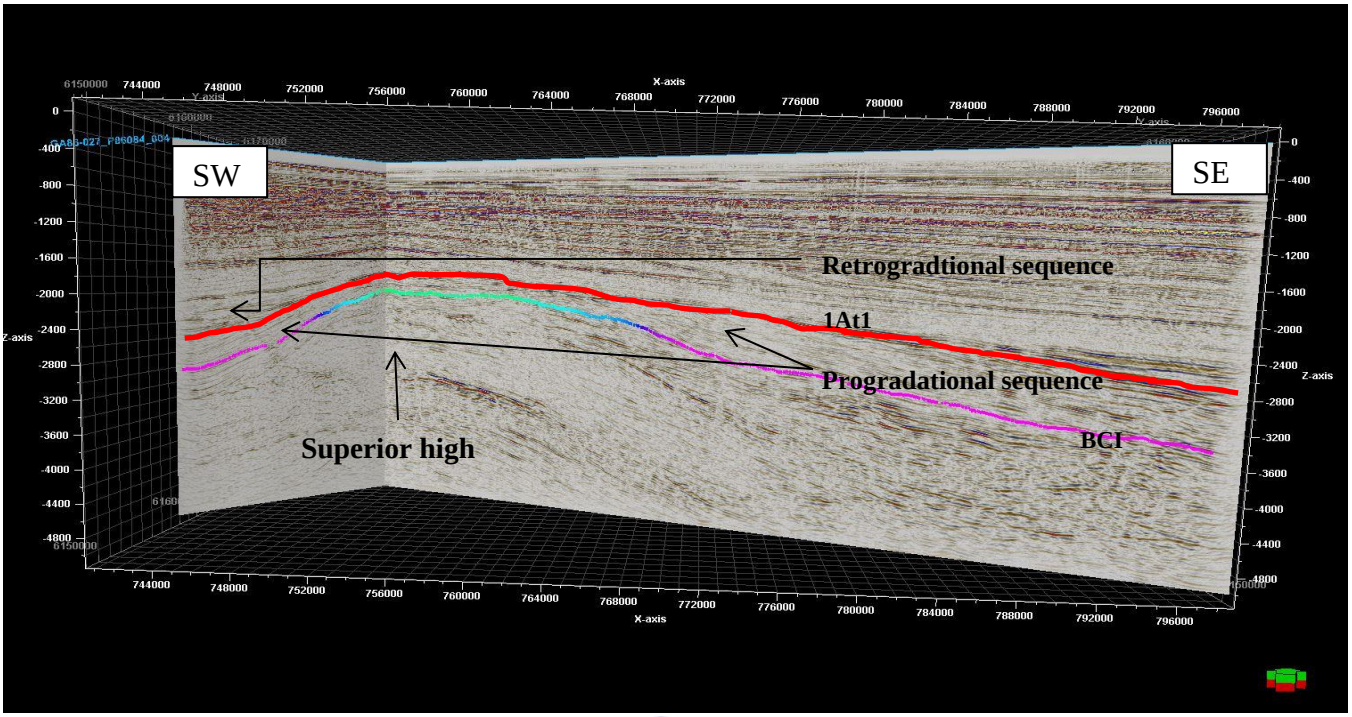

Figure 4.3.3: Progradational and retrogradtional sequences in the southern most section of the study area in the Pletmos basin.

The Outeniqua basin is known to be tectonically controlled by its basement highs (McMillan, et al., 1997). The Pletmos basin is therefore also highly influenced by its pre-Mesozoic basement, which resulted in many structural highs being formed due to the uplift of this basement caused during rifting, figure 4.3.3 illustrates, and sedimentation that was deposited forms a lens like architecture.

This structural high is known as the superior high. A divergent internal reflection pattern is seen in the wedge to lens like shaped unit (figure 4.3.3) which could be interpreted as a result of lateral variations in the energy of deposition or progressive tilting of the sedimentary facies during deposition.

The interval between the 1At1 and BCI as shown by the late Jurassic to Early Cretaceous synrift I progradational sequence that can be seen (figure 4.3.3.) with sigmoidal internal configuration, this progradational sequence shows thickening towards the SW and towards the SE. The progradational sequence is followed by a retrogradtional sequence indicating the start of the transgressive period.

4.4 Petrophysical analysis

4.4.1 Introduction

Petrophysical analysis was conducted on three wells Ga-A3, Ga-Q1 and Ga-Q2. Each reservoir has a percentage of shale or clay ranging between 45% -50% which could cause an certain amount of error for the water saturation and porosity derived from the logs. The aim was to calculate the Vclay, permeability and water saturation of zones A and B. The core data that was obtained from the conventional core analysis i.e. porosity, permeability and water saturation was used to calibrate with the calculated porosity logs and permeability logs.

According to Crain (2001) a petrophysical analysis is done in order to obtain more knowledge about the reservoir section. Especially for the evaluation of the well logs, to obtain the fluid properties as well as the porosity, permeability and lithology this is usually correlated to the core.

4.4.2 Well Ga-A3 Interpretation

In Well Ga-A3 (figure 4.4.5.1), zone A is situated at depth of 1679m to 1705 and zone B at 1734m to 1786m. **In track 1:** the gamma ray log (GR), a base line of 85 API was applied to well Ga-A3, Zone A, shows a fining upward sequence topped by a clay unit. Zone B becomes more sandy than zone A, revealing three 5m sandstone units each separated by silt and clay units. **In track 2:** the composite log suite of neutron/density (NPHI/RHOB) displays in zone A no crossover to indicate possible hydrocarbon. However zone B at a depth of 1758m to 1760m shows possible water bearing zone which is indicated by the crossover of NPHI/RHOB.

In track 3: Deep resistivity (ILD), deflects slightly to the left at the depth of 1758 to 1760m zone B. **In track 4:** Permeability (K), displays a good match between the calculated permeability and the permeability measure from the core data, permeability ranges from 0.1mD to 6.5 mD indicating fair permeability (table 3.2.3-1), in zone B a slight decrease in permeability, whereby permeability descends just below 1mD in the hydrocarbon zone.

In track 5: the calculated water saturation (Sw) and the residual fluid saturation from the core analysis matches the Indonesia saturation (SwInd) curve in zone A and zone B. At the interval of 1758m -1760m water saturation increases to 100%. The relationship between Sw

and ILD shows that as the Sw averages to 70% at the top of the well log, the ILD tends to decreases. Further down on the well log the Sw increases to about 100% and the ILD decreases in correspondence to the increase in water saturation of the well bore.

In track 6: Density porosity (PhiDen) and effective porosity shows a good match with the log data and the core data porosity ranges from 1% to 19% which is expected for very fine sandstone. Porosity decreases substantially at the depth of 1759m to 1%. **In track 7:** Volume of clay (VCLGR) shows about 40 to-50% volume of clay in zone A and in Zone B in the three sandstone units it decreases to about 10%.

4.4.3 Well Ga-Q1 Interpretation

In Well Ga-Q1 (figure 4.4.6.1), zone A is situated at a depth of 2288m to 2348m and zone B at a depth of 2405m -2455m. **In track 1:**(GR), a base line of 85 API was applied, two coarsening upward sequences have been identified in zone A. In zone B four major sandstone units are identified. **In track 2:** (NPHI/RHOB), shows a possible gas zone at a depth of 2322m to 2326m in zone A and in zone B at a depth of 2432m to 2340m another gas zone.

In track 3: (ILD, MSLU, SFLU), at the depth of 2432m to 2340m clear separation of the resistivity logs indicates that this zone could contain gas, although just above it the resistivity log increases which is as a result of the Rmf being greater than the Rw. **In track 4:** (K), good match core samples and between the calculated effective permeability, permeability ranges from 1mD to 6mD at the hydrocarbon zone B a decrease in permeability is noticed.

In track 5: (Sw), a good match between the core water saturation and the calculated water saturation is identified, throughout zone A with 60% water saturation at the gas zone decreases to about 45-50% and zone B about 60% water saturation, with the hydrocarbon zone in zone B showing an increase water saturation.

In Track 6: (PhiDen), effective porosity and the core analysis shows a good match, porosity ranges from 6% to 21%, an increase in porosity is noticed in zone B. **In track 7:** (VLCLGR), zone A displays about 45% to 50% volume of clay, Zone B also displays this trend except for in the hydrocarbon zone where volume of clay decreases to about 10%.

4.4.4 Well Ga-Q2 Interpretation

In well Ga-Q2 (figure 4.4.7.2) zone A is found at depth of 2264m to 2399m and zone B at a depth of 2416m to 2462m. **In track 1:** (GR), a baseline of 86 API was applied. Zone A comprises of four major sandstone units separated by 1m clay units respectively and zone B comprises of three major sandstone units.

In track 2: (NPHI/RHOB), zone B at a depth of 2452m – to 2460m, the NPHI/RHOB shows a possibility of hydrocarbon. **In track4:** (ILD, MSLU, SFLU), has significant responses in the resistivity log is observed at the depth of 2452m – 2460m, the resistivity logs indicate possible gas in zone B.

In track 5: (Sw), the Indonesian model of Sw was applied. This leads to a high trend 60 – 80% of Sw throughout the zones A and B. Particularly in the gas section in zone B an decrease in Sw to about 50% is observed as the ILD decreases. **In Track6:** (PhiDen), indicates a porosity of 14- 19% in the gas are of zone. **In Track 7:** (VCLGR), displays a 35% volume of clay in zone A and increase in zone B whereby the volume of clay increases to 50%.

4.4.5 Well Ga- A3 well log

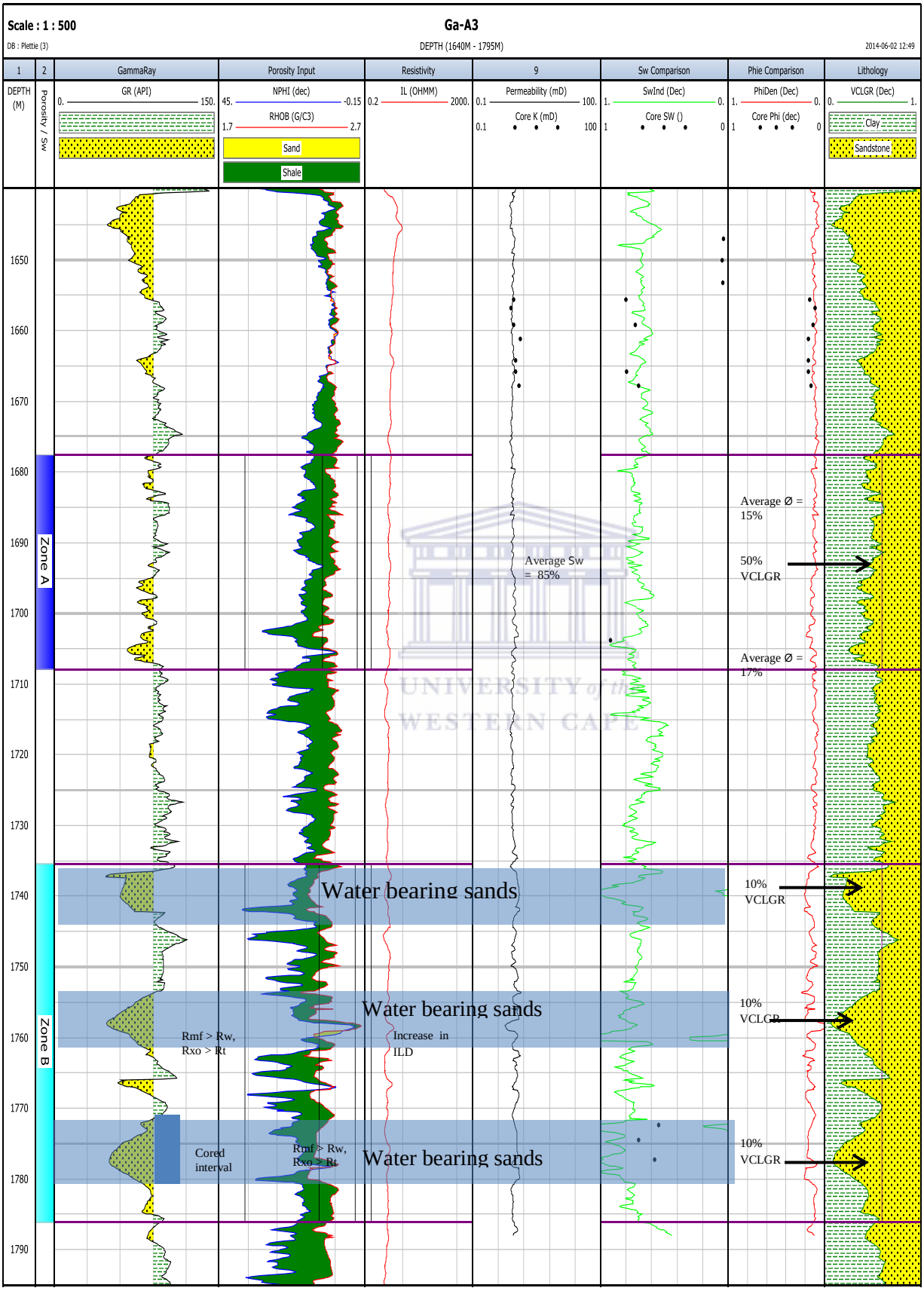

Figure 4.4.5.1: Plot of well Ga-A3 showing a petrophysical properties of reservoir calibrated with the core analysis of porosity and permeability, including the invasion profiles.

4.4.6 Well Ga-Q1 well log

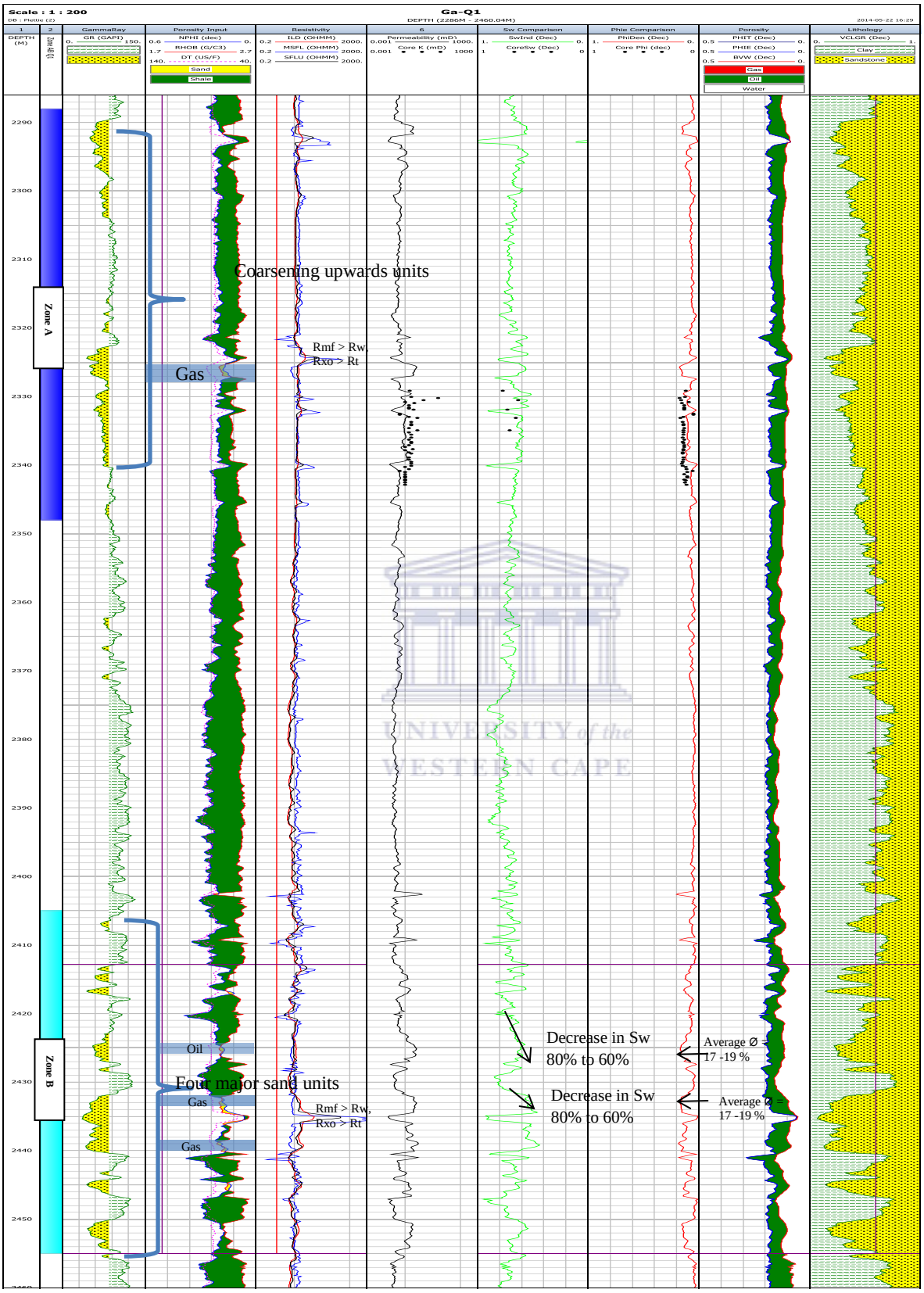

Figure 4.4.6.1: Plot of well Ga-Q2 showing a petrophysical properties of reservoir calibrated with the core analysis of porosity and permeability, including the invasion profiles.

4.4.7 Well Ga-Q2 well log

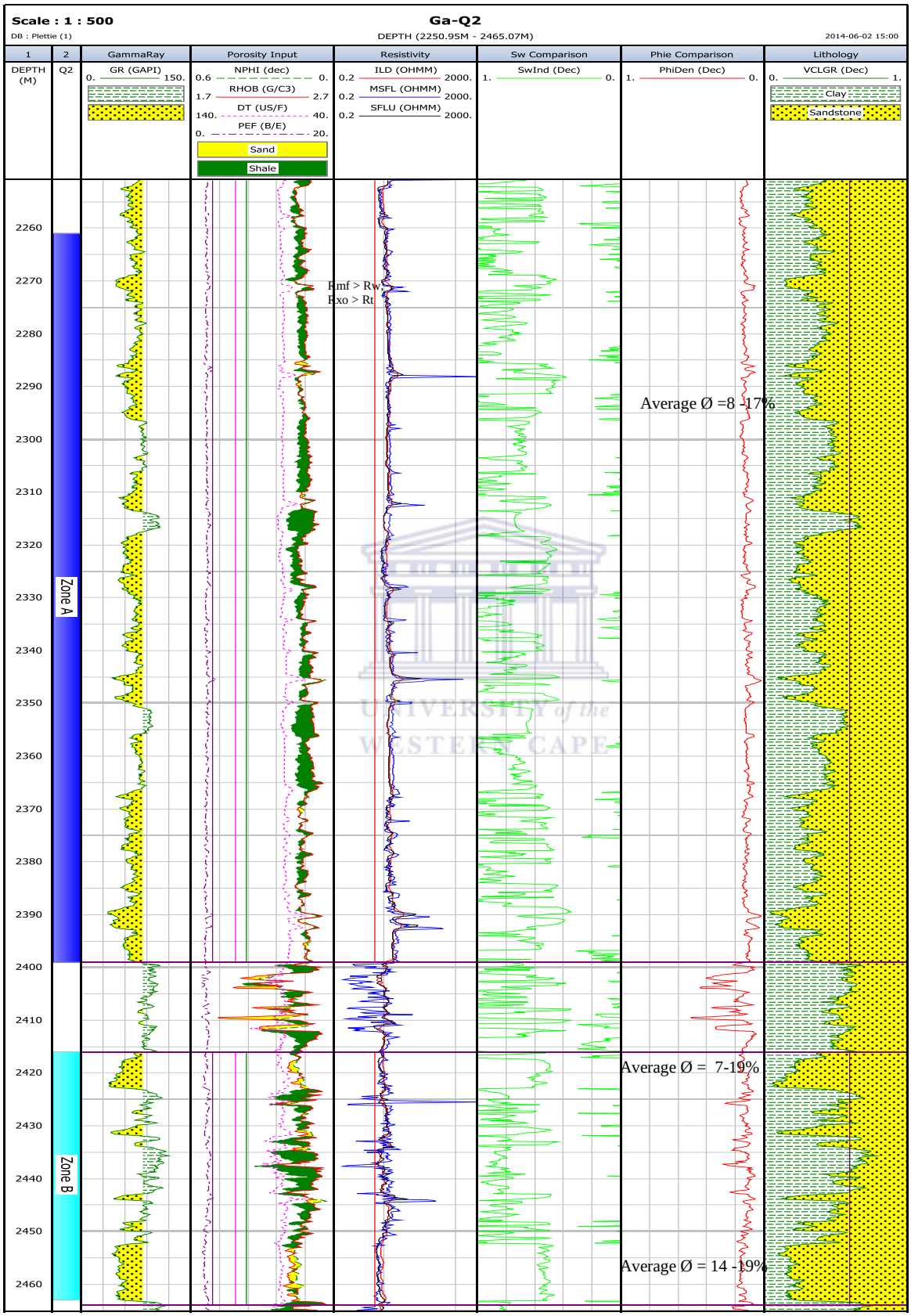

Figure 4.4.7.1: Plot of well Ga-Q2 showing a petrophysical properties of reservoir calibrated with the core analysis of porosity and permeability, including the invasion profiles.

4.4.8 Petrophysical parameters and the sedimentary logs.

4.4.8.1 Well Ga-A3

Petrophysical parameters such as porosity and permeability are displayed next to the sedimentary logs of the cored zone in figure 4.4.8. The porosity and permeability of this cored zone at a depth of 1777m has been influenced by the facies A4 whereby the calcite cementation is a possible cause for the reduction of porosity and permeability of this zone.

4.4.8.2 Well Ga-Q1

Based on (figure 4.4.8.2,) porosity and permeability (table 4.4.8 1), is affected strongly by facies B1 where intense bioturbation has deteriorated the permeability

Facies	Porosity %	Permeability mD
A1	16-17	1
A2	16 -17	1
A3	10 - 17	0.1 – 1
A4	9 - 11	0.8 – 0.9
B1	2-5	0.2-0.4
B2	7-10	0.7 - 1
B3	10	0.1-1

Table 4.4.8-1. Facies associated with the petrophysical properties (average porosity and average permeability).

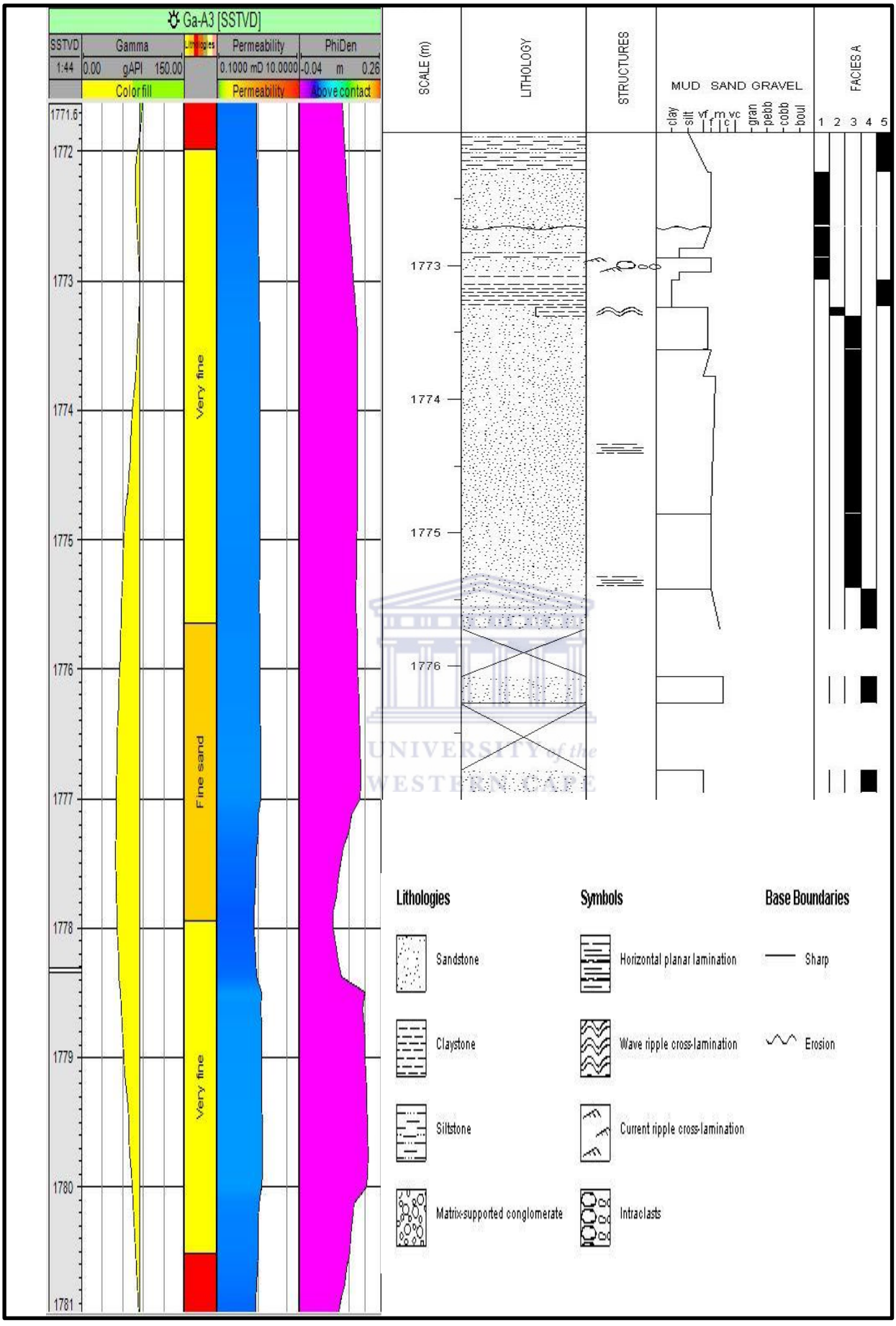

Figure 4.4.8.1: Well Ga-A3 displaying the core interval lithology alongside permeability(K) and effective porosity (PhiDen).

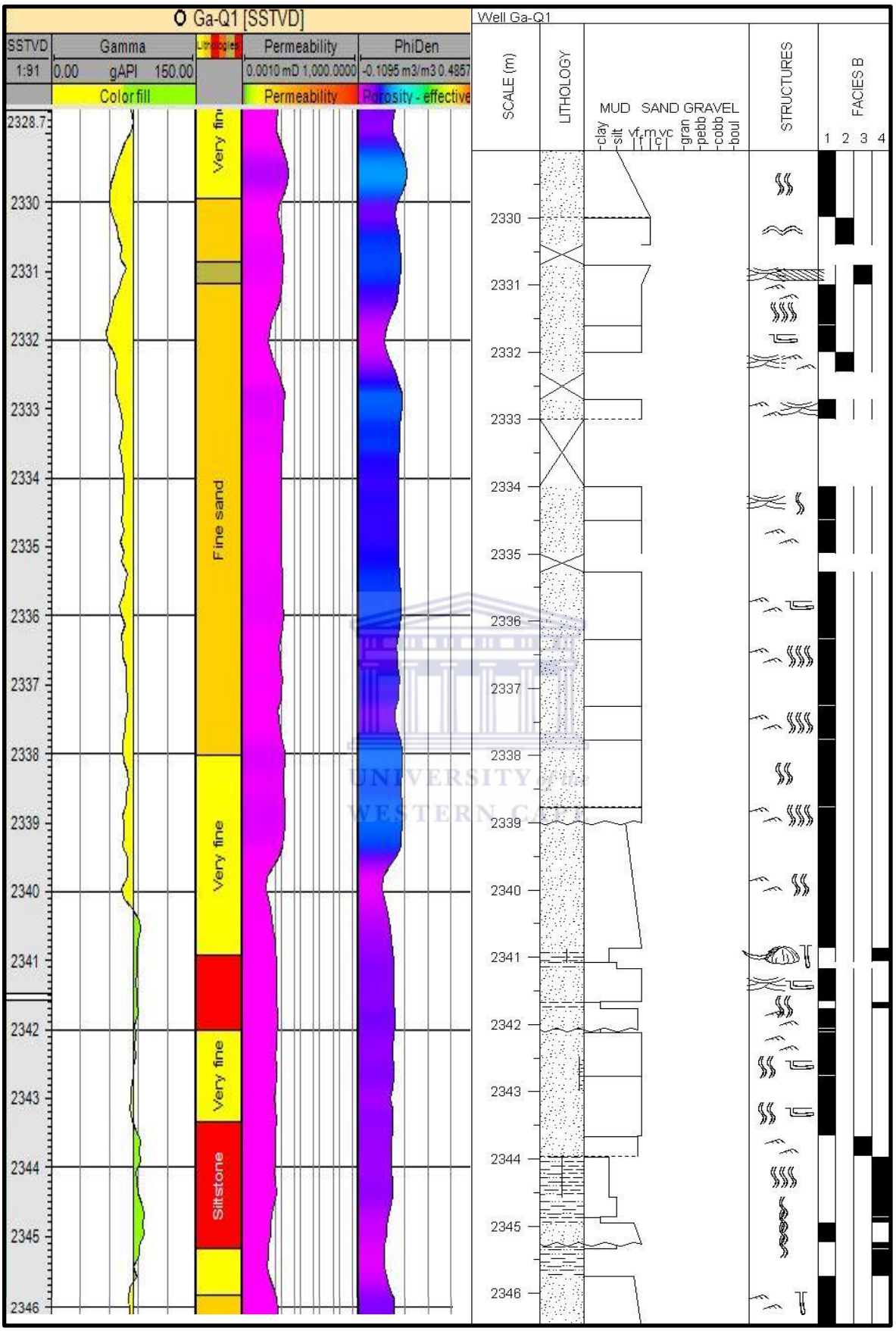

Figure 4.4.8.2: Well Ga-Q1 displaying the cored interval lithology alongside the versus the effective permeability (K) and effective porosity (PhiDen).

4.5 Geomodelling

4.5.1 Velocity model

The figures below shows the QC process which is part of the result of the depth conversion of the seismic, After creating a time depth relationship of the wells, a velocity model was generated using the linear velocity algorithm, the uncorrected data is shown in figure 4.5.1 and the corrected data figure 4.5.1.2.

Figure 4.5.1: Linear plot of interval velocity against two way time.

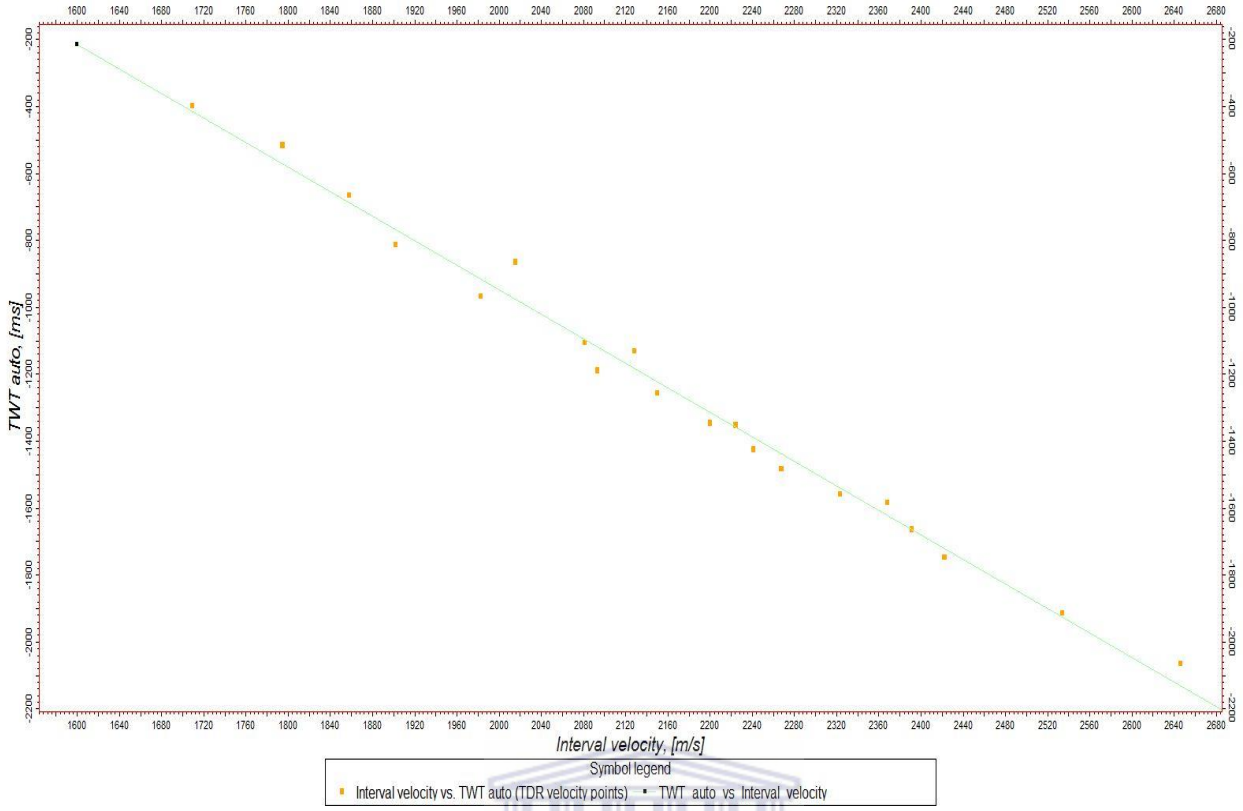

Figure 4.5.1.1: Linear plot of interval velocity against two way time.

4.5.2 Upscaling

Lithological facies between the BCII - BCI (figure 4.5.2) shows logs at the top of the figure before upscaling was applied. Wells Ga-A3, Ga-Q1 and Ga-Q2 at the bottom of figure 4.5.2 show the modelling results after applying the stochastic algorithm (SGS); whereby sampling values from well logs or well log attributes were extrapolated into the grid.

During the realisations well Ga-A3 was biased to be more clayey than well Ga-Q1 and well Ga-Q2. Well Ga-Q1 and Ga-Q2 had a proportionate ratio of sandstone to clay. This was done to preserve the heterogeneity of the reservoir zone A and zone B; which the trends could be seen by the thickening of the sandstone units in well Ga-Q1 and Ga-Q2.

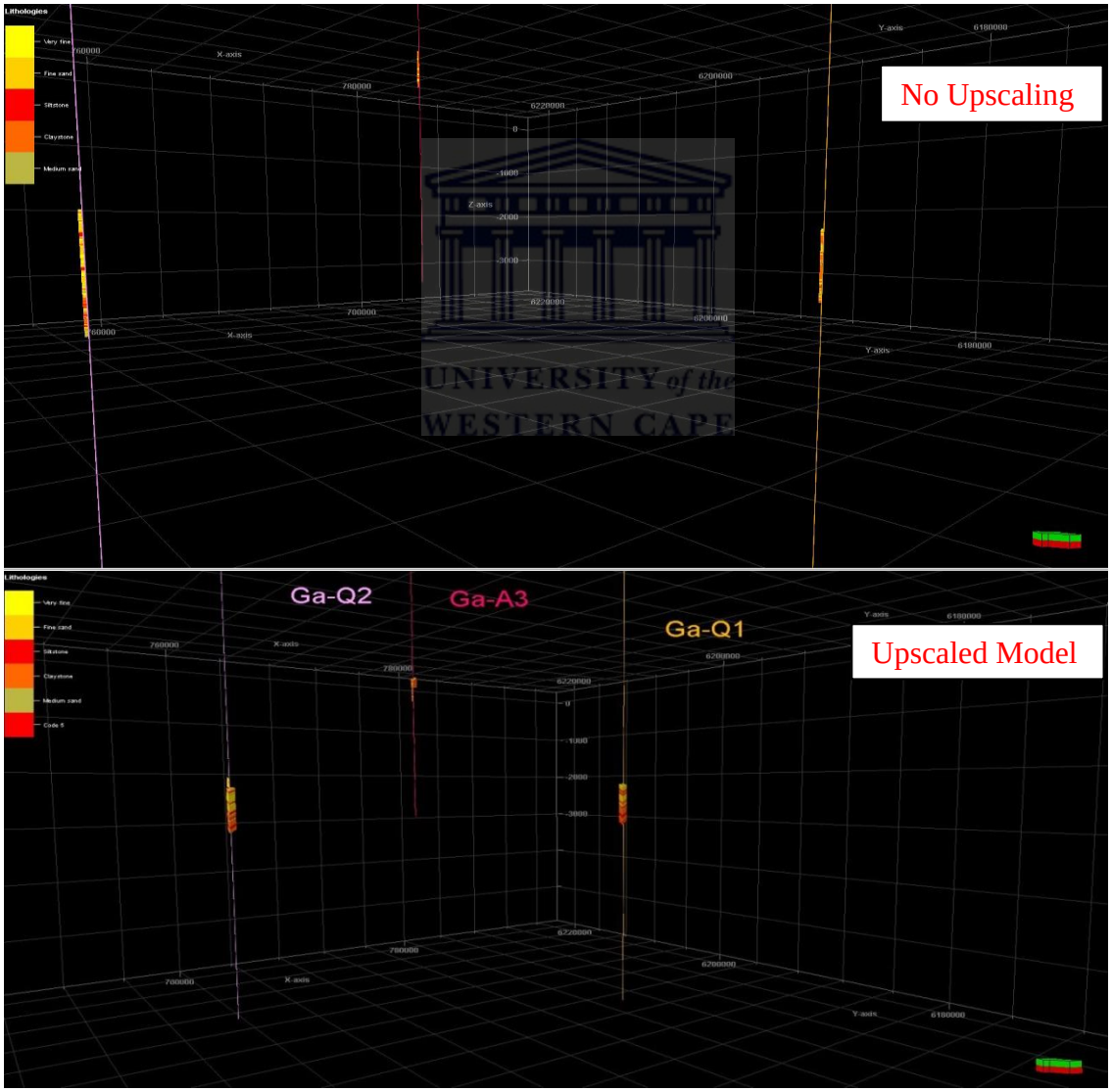

Figure 4.5.2: Lithological logs at the top of the figure have not been upscaled whereas the well logs at the bottom of the figure have been upscaled.

4.5.3 Property Modelling

The property modelling comprised of several realisations to show the distribution trend of the lithofacies that were generated by applying the stochastic method (SGS).

Realisation 1: (Figure 4.5.3), displays a facies trend where a regional increase in clay trend was imposed. The high clay intervals that separate the clastic reservoir units in zones A and B could represent possible barriers between the sandstone units. These claystone units thicken towards the west of Ga-Q2 and east of Ga-Q1.

Realisation 2: (Figure 4.5.3), shows an increase in siltstone and claystone content which thickens towards the west of Ga-Q2 and east of Ga-Q2. This increase in clay content could be a possible factor that could influence the vertical and horizontal fluid movement.

Realisation 3: (Figure 4.5.3), indicating a bias towards the sandstone units within the area, where the very fine grained sandstones have been simulated to 19%, fine grained sandstones 25% , medium grained sandstone 7%. This realisation indicated a thickening of the sandstones to west of Ga-Q2 and thickening towards the east of Ga-Q2. The medium grained sandstones displays a thickening trend towards the east and north shown in figure 4.5.3. A noticeable trend towards the north of well Ga-A3 and east of well Ga-Q1 is an increase in medium grained sandstones indicating an increase in coarser sediment which could be interpreted as an increase in the energy of the deposition of the sediments.

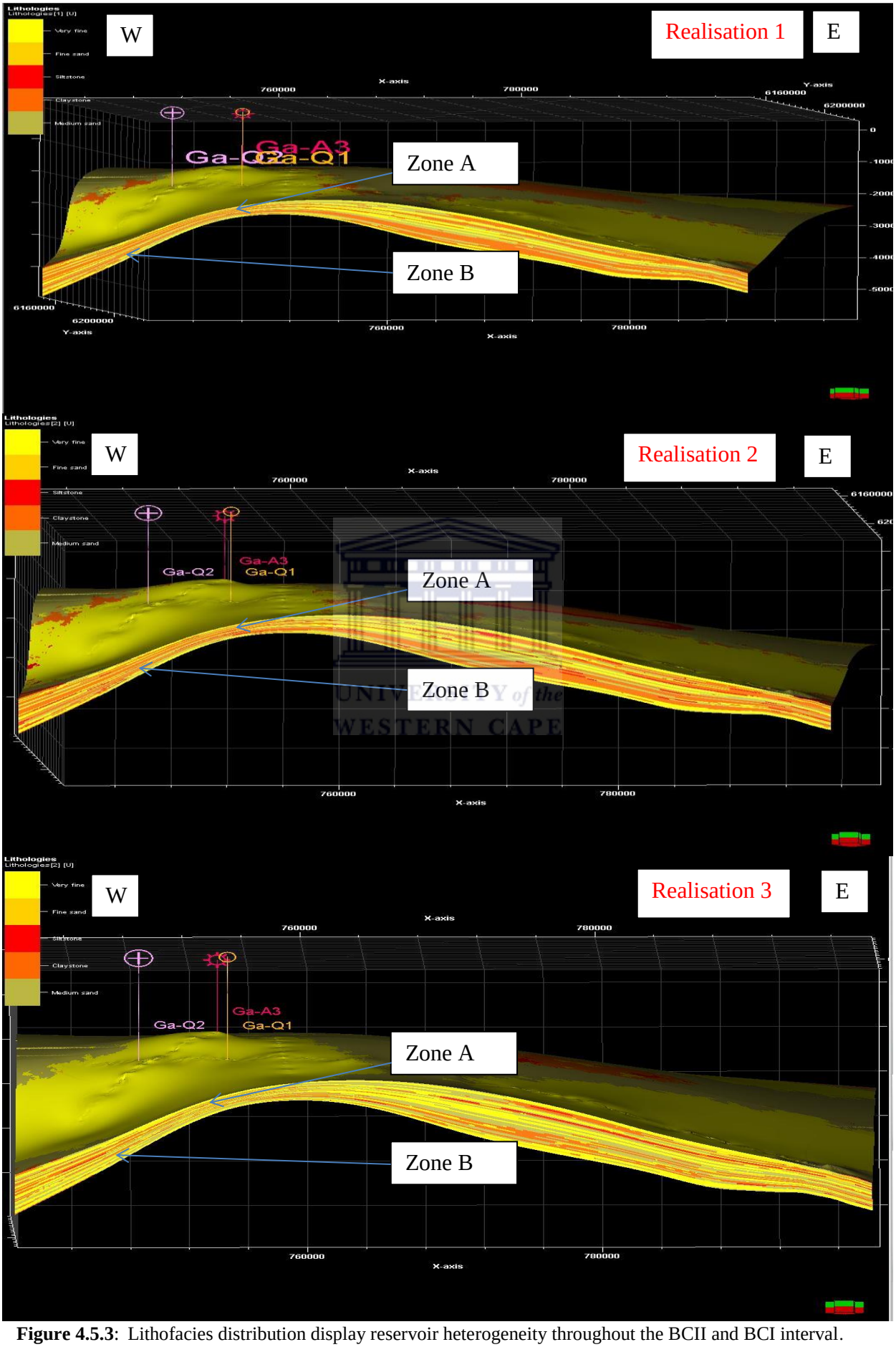

Figure 4.5.3: Lithofacies distribution display reservoir heterogeneity throughout the BCII and BCI interval.

4.5.4 Petrophysical Modelling

Petrophysical modelling was done by applying the stochastic algorithm (sequential Gaussian simulation). This was done to extrapolate the porosity and permeability distribution trends away from the well bore. Wells Ga-A3 and Ga-Q1 had there permeability and porosity logs determined from the core analysis calibrated with the calculated logs respectively. Well Ga-Q2 did not have such a analysis applied to it, but through petrophysical modelling, a possible trend of porosity and permeability can be predicted.

Applying the same method for porosity (figure 4.5.4.1) displays an average porosity of 10% being applied around the wellbores of Ga-A3 and Ga-Q1. The trend distribution data suggest that the porosity around the vicinity of well Ga-Q2 will decrease to an average of 5%, but on the flanks of the structural high, porosity varies between 5 and 10%.

In figure 4.5.4.2 an average porosity of 15% was applied around well Ga-A3 and Ga-Q1. The trend distribution observed around the Ga-Q2 averages around 10% porosity. Towards the east of well Ga-Q1 the trend distribution map shows a high anomalies of porosity reaching about 25%. Yellow spots can be related to geomodelling artefacts as the regional trend of porosity ranges between 15 to 25% whereas the artefacts indicate a porosity of 30-40%.

Realisations were computed for permeability (figure 4.5.4.3) used an average permeability of 0.8 mD staying within the average permeability that has been identified within well Ga-A3 and Ga-Q1. A trend can be observed that surrounding the wells of Ga-A3 and Ga-Q1 the average of 0.8mD has been maintained. Towards Ga-Q2 the permeability trend decreases towards 0.5mD as an average permeability for well Ga-Q2 further west of well Ga-Q2 permeability decreases to about 0.1 to 0.3 mD. As prediction several high and low permeability zones can be expected within the well bore of Ga-Q2.

An increased averaged (figure 4.5.4.4) of 4mD was taken for well Ga-A3 and Ga-Q1 based on the possibility that permeability might increase towards well Q2. A trend is observed that towards well Ga-Q2 the permeability tends to average between 1mD- 5mD. Following a westward trend from well Ga-Q2 permeability begins to decrease to about 0.9mD.

Simulations done at an average of 5mD indicated an erroneous result as the clay barriers were not being acknowledged by the model.

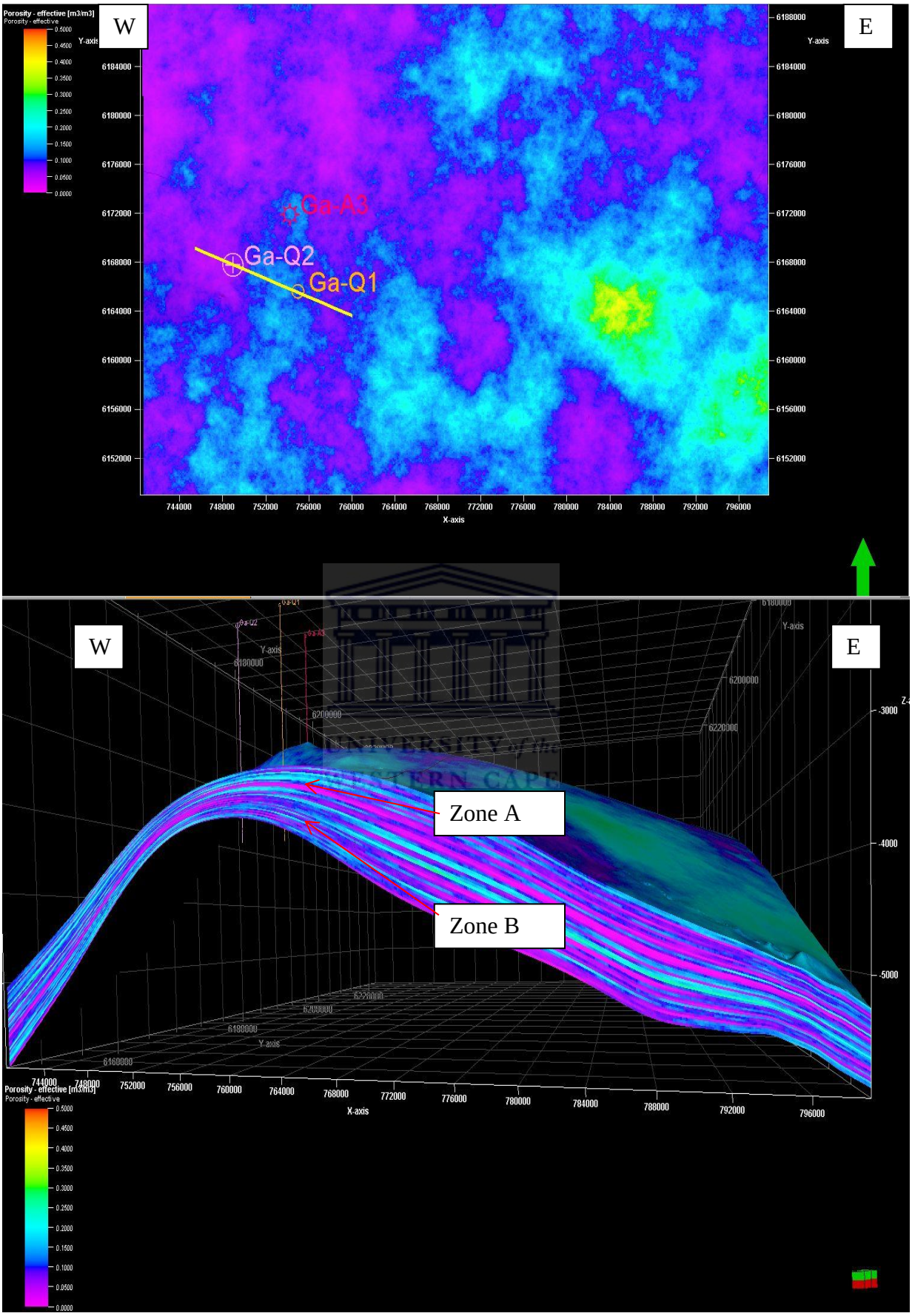

Figure 4.5.4.1 Porosity simulated to an average of 10% around the wellbores.

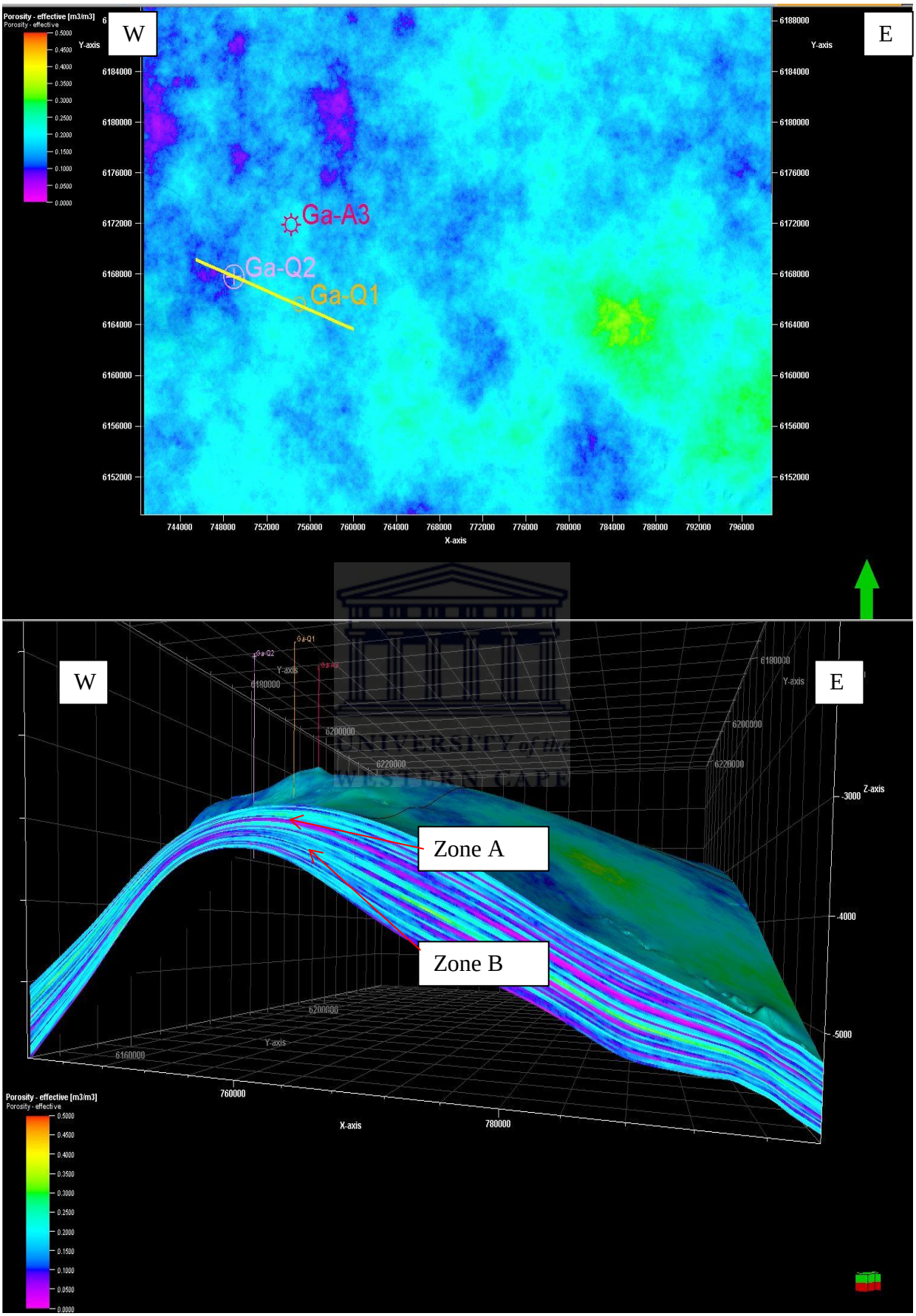

Figure 4.5.4.2 Porosity simulated to an average of 15% around the wellbores.

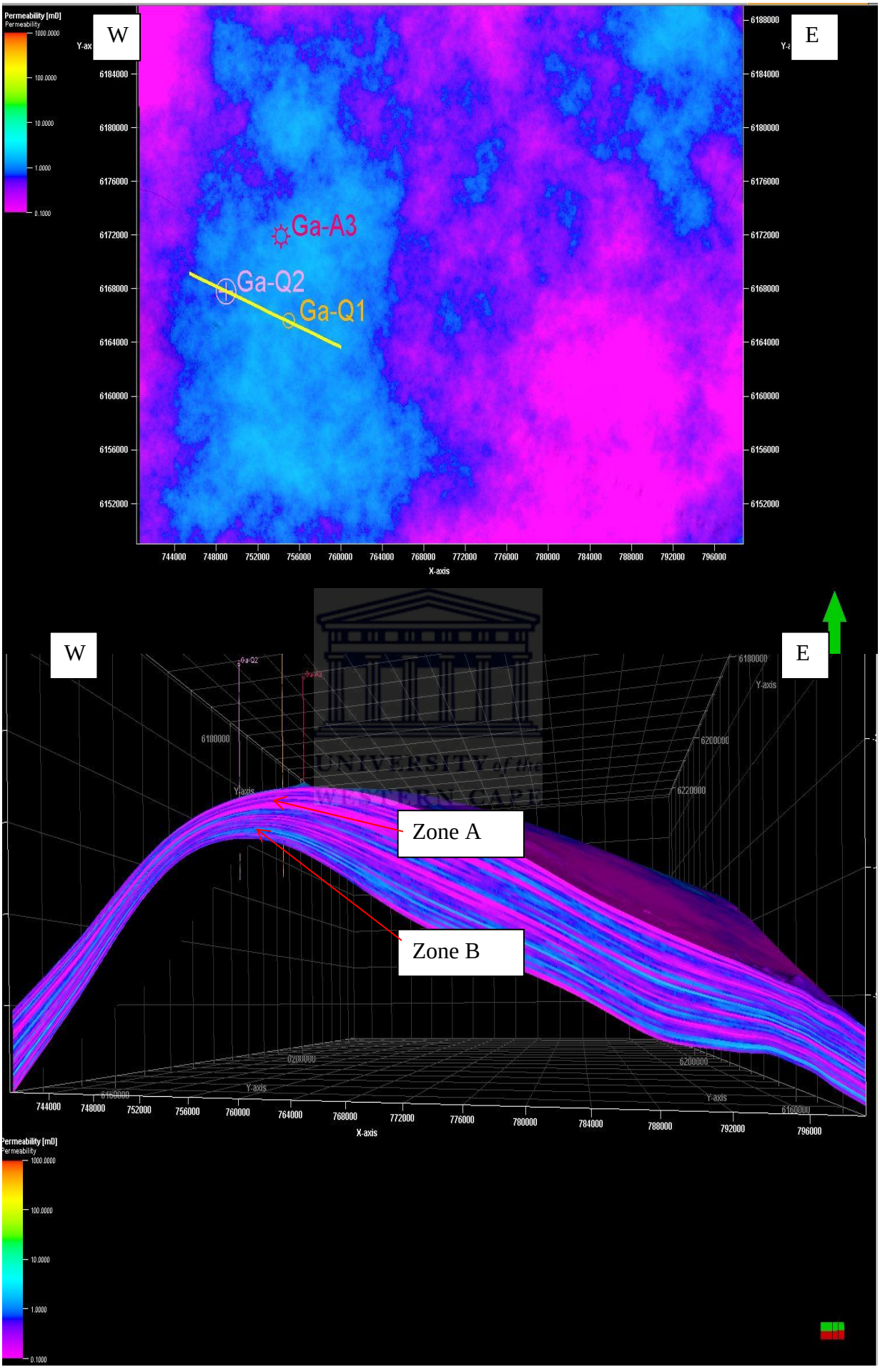

Figure 4.5.4.3 Permeability simulated with an average of 0.8 mD around the wellbores.

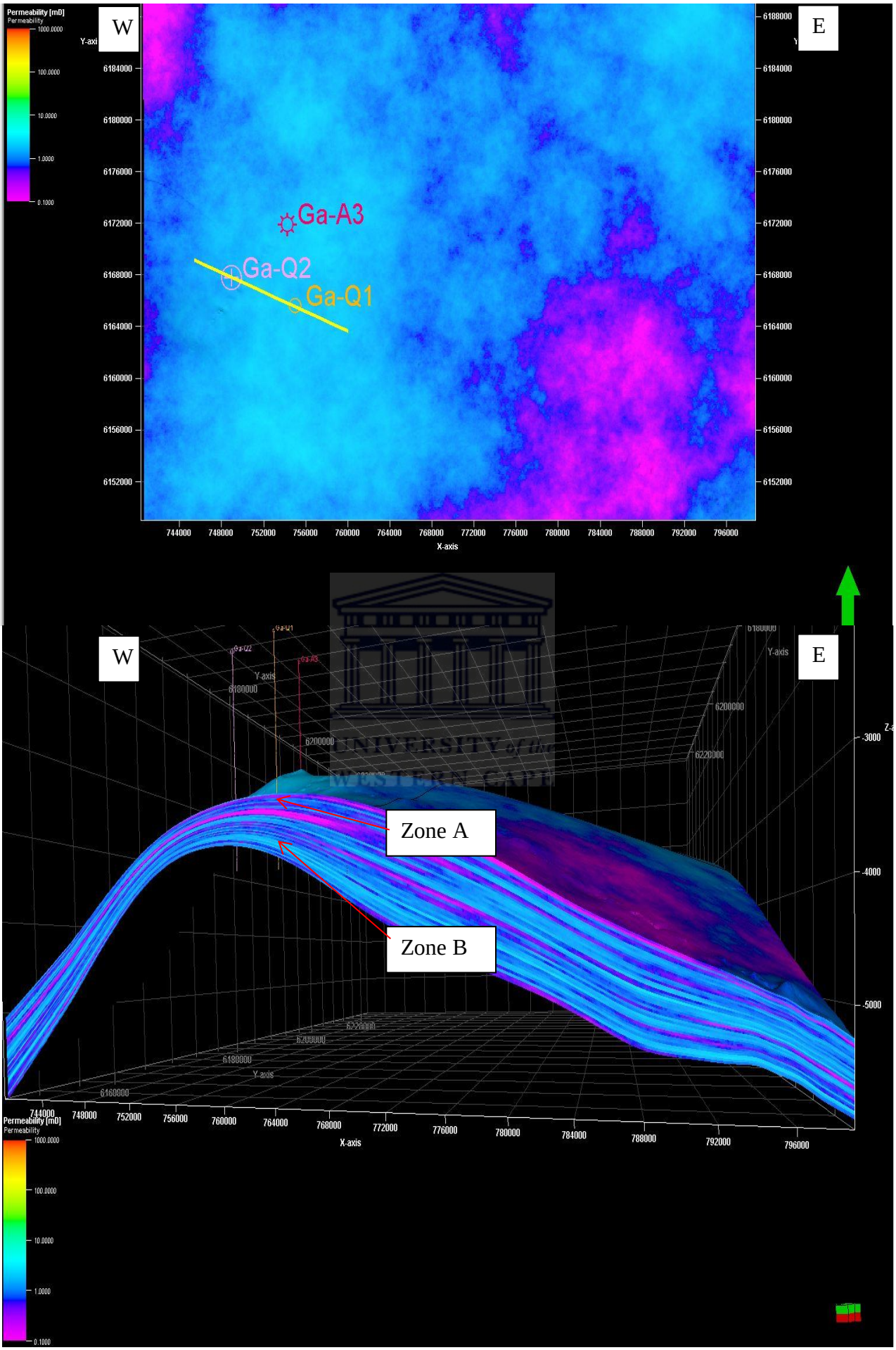

Figure 4.5.4.4: Permeability simulated at an average of 4mD around the wellbores.

Chapter 5:

5. Discussion

The influence of the structural high on the geometry of the reservoir is evident in the way the synrift I sedimentation was deposited in a lens like architecture. The facies and core results indicate the effect of second order depositions cyclic sequences which were active during the deposition of the synrift sediments. Small scale heterogeneity is observed in the sediments of BCII to BCI, which is related to the sedimentary structures that are present within the sandstones and that was identified in the cores of the reservoirs zones of interest.

Small scale heterogeneity was also identified during the transition from one rock lithology to another according to McCarthy (1991) grain size can be accounted for by a straight forward averaging method, this was accounted for during the simulation of the model. Large scale heterogeneity was displayed in the lithological models as was the claystone barriers identified as potential baffles and good reservoir seals due to their wide later extent across the study area. In petroleum modelling several acknowledgments have been made, that small scale heterogeneity and large scale heterogeneities plays a vital role in hydrocarbon recovery. Although it must be highlighted that secondary diagenetic changes have an effective control of the heterogeneities on an intermediate scale.

Comparison between sedimentary structures, porosity and permeability indicates the influence of the small scale (i.e. clay lenses, bioturbation) has on the control of porosity and permeability. Whereby sandstones units that were facies unit B, where highly bioturbated sandstones have been interpreted and distinct mud draping laminae showed a decrease in permeability compared to the cleaner sandstone units. The internal structure mud drapes are thin layers of mud covering the seafloor during the turning of tide (Houthuys, 1990).

The lithofacies distribution indicates a lagoon to beach environments in well Ga-A3 and Ga-Q1, and grades into proximal marine in well Ga-Q2. Simulation data suggests an increase in thickness of the sediments or sandstone reservoirs units on the flanks of the structural high. McMillan suggests that the variable lithology's of thick sandstone units with the transgressive clays, were deposited mainly in the graben and reflect rapid changes in depositional environment.

In addition to the depositional environments, the porosity distribution of the siliciclastic reservoir sandstones and the variability of the permeability distribution could influence the reservoir drainage. While the permeability is directly related to porosity, it can also be affected considerably by the presence of claystone (McCarthy, 1991).

Chapter 6

6. Conclusion:

The reservoir heterogeneity of the sandstones of the BCII- BI interval have been well defined within the framework of this research, in accordance to the aims and objectives which was stipulated at the beginning of this thesis. There might be some uncertainty in the geological model as the faults of the structural framework that could not be honoured in the geological model due to software limitations. Although through the specific application of sequential gaussian algorithm in the stochastic modelling this ensured that all of the available data was honoured to the highest extent in generating the multiple realisations

In conclusion the studied reservoir zones A and B of each of the three wells namely well Ga-A3, Ga-Q1 and Ga-Q2 falls within the BCII to BCI interval of the shallow marine Synrift I sediments. Structural highs have been identified as a major influence on the deposition of the sediments and geometry of the reservoir zones. Small scale reservoir heterogeneity has been construed to the influence of the sedimentary structures (bioturbation and bedding) and the effect of grain size it has on the porosity/permeability on a small scale. Large scale reservoir heterogeneity has been identified, due to the lateral extent of the claystones which is widely distributed throughout the study area.

6.1 Recommendations:

In the future the following could be considered for a better understanding of the heterogeneity:

- Due to the varying sedimentation during the deposition of the synrift I sediments a petrographic study will reveal the influence of diagenesis on the reservoir heterogeneity on a micro scale.
- History matching with surrounding wells should be done, to observe the contrast in flow during production test.
- Numerical flow simulation of the migration of the different phases of hydrocarbon can be used to identify the actual behaviour of the reservoir under production (McCarthy, 1991).

7. Bibliography

Aguilera, R., 2004. Intergration of geology, petrophysics, and reservoir engineering for characterization of carbonate reservoirs through Picket plots. AAPG Bulletin, Volume 88(doi: 10.1306/12010303071), pp. 433-446.

Blackbourn, G., 1990. Cores and core logging for geologists. s.l.:Whittles Publishing .

Bond, C., Gibbi, A., Shipton, Z. & S., J., 2007. What do you think this is? "Conceptual uncertainty" in geoscience interpretation.. GSA Today, 17(11), pp. 4-8.

Broad, D., Junslager, E., Mclachlan, I., Roux, J., 2006. Offshore Mesozoic Basins. In: Johnson, M.R. et al, The Geology of South Africa: Geological Society of South Africa. Pretoria: Johannesburg/Council for Geoscience, pp. 553 - 571.

Brown, L.F., Benson, Jr., M., Brink, G.J., Doherty, S., Jollands, A., Junslager, E.H.A., Keenan, J.H.G., Muntingh, A., and Van Wyk, N.J.S., 1995. Sequence Stratigraphy in Offshore South Africa Divergent Basins: An Atlas on Exploration for Cretaceous Lowstand Traps by Soeker (Pty) Ltd.. AAPG studies #41 ed. Tulsa, Oaklohoma, 74101, USA.: The American Association of Petroleum Geologist.

Crain, E., 2001. Crain's Petrophysical Handbook. [Online] Available at: http://www.spec2000.net/14-swbasics.htm [Accessed 23 January 2014].

De Wit, M.J., Bowring, S., Ashwal, L.D., Randrianasolo, L.G., Morel, V.P.I., 2001. Age and tectonic evolution of Neoproterozoic ductile shear zones in southwestern Madagascar, with implications for Gondwana studies. Tectonics, Volume 20, pp. 1-45.

Dingle, R., Siesser, W., and Newton, A., 1983. Mesozoic and Tertiary GeoMesozoic and Tertiary Geology of Southern Africa: A Global Approach to Geology. Rotterdam: Taylor & Francis.

Douglas, G. P. et al., 1992; . Measuring and Predicting Reservoir Heterogeneity in Complex Deposystems (The fluvial Deltaic Big Injun Sandstone in West Virginia). Fossil Energy, Volume DOE/BC/146571-11 20 September, pp. Pg1-5.

Glover, M., 2000. Petrophysics MSc Class notes, United Kingdom: Department of Geology and Petroleum Geology, University of Aberdeen..

Johnson, C. and Greenkorn, R., 1963. Description of gross rock heterogeneity by the correlation of lithologic and fluid properties from core sampes.. International Association of Scientific Hydrology., Bulletin, 8:3(DOI: 10.1080//02626666309493337), pp. 52-63.

Larsen, R. and Ladd, J., 1973. Evidence for the Opening of the South Atlantic in the Early Cretaceous.. Nature, V246, pp. 209-212.

Marty, B., Dewonck, S., and France-Lanord, C., 2003. Geochemical evidence for efficient aquifer isolation over geological timeframes. Nature, 425(9), p. 55–58.

McCarthy, J., 1991. Analytical models of effective permeabilty of sand-shale reservoirs.. Geophysical Journal International, 105(2), pp. 513-527.

McMillan, I., 2003. Foraminiferally defined biostratigraphic episodes and sedimentation pattern of the Cretaceous drift succession (Early Barremian to Late Maastrichtian) in seven basins on the South African and southern Namibian continental margin : research article. South African Journal of Science, Volume 99(Issue 11 & 12), pp. 537-576.

Mcmillan, I., Brink, G., Broad, D., and Maier, J., 1997. Late Mesozoic Sedimentary Basins off the South Coast of South Africa. Sedimentary Basins of the World, Volume 3(1874-5997), pp. 319-376.

Mitchum, R. M., Vail, J. P. R., and Thompson, S., 1977. Seismic stratigraphy and global changes in sea level, part 2: the depositional sequence as basic unit for seismic stratigraphic analyses, in C.E. Payton, ed.. Seismic Stratigraphy - Applications to hydrocarbon exploration., III(AAPG Memoir, 26), pp. 53-62.

Neal, J., Risch, D. & Vail, P., 1993. Sequence stratigraphy- A Global Theory for Local Success, s.l.: Schlumberger, Oilfield Review.

Nichols, G., 2009. Sedimentology and Stratigraphy. Second Edition ed. West Sussex, United Kingdom: Blackwell Publishing.

PASA, 2010. Barremian Prospects of the Northern Pletmos Basin. [Online] Available at: http://www.petroleumagencysa.com/images/pdfs/Northern_Pletmos_Basin.pdf [Accessed 28 March 2014].

PASA, 2013. Petroleum Agency South Africa., History of exploration and production. [Online] Available at: www.petroleumangecysa.com/index.php/petroleum-geology-resources/exploration-history [Accessed 28th March 2014].

Petford, N. and Mc Caffrey, K., 2003. Hydrocarbons in crystalline rocks .. Special Publication 214, 248p ed. London: Geological Society Publishing House.

Rider, M., 1996. The Geological Interpretation of Well logs.. 2nd Edition ed. Scotland, Caithness: Whittles Publishing.

Roux, J., 1997. Potential outlined in Southern Outeniuqua off S.Africa. Oil & Gas Journal, Volume 95(25).

Roux, J. and Davids, A., 2010. Barremian Basin Floor Fan Complex: An Untested Gas Play within the Northern Pletmos Basin. Search and Discovery Article: AAPG International Conference and Exhibition, Rio de Janerio, Brazil, November 15-19, 2009., Issue #10234.

Schlumberger, 2006. Reduced drilling risk with 3D surface seismic data.. Reservoir Heterogeneity Study Improves Well Planning Efficiency Case study:, pp. 1-2.

Schlumberger, 2013. Petrel E&P Software Platform 2013.1:Schlumberger.

Scotese, C., 2002. Plate tectonic maps and continental drift animations. [Online] Available at: http://www.scotese.com. [Accessed 12 February 2014].

Selley, R., 1978. The book titled Ancient Sedimentary Environments.. 131-151 ed. Netherlands: Springer .

SEPM. & Geololgy., S. f. S., 2013. sepmstrata. [Online] Available at: http://www.sepmstrata.org/page.aspx?pageid=410 [Accessed 03 March 2014].

SPE, I., 2013. Petrowiki. [Online] Available at: www.petrowiki.org/Estimating_permeability_from_well_log_data [Accessed Janaury 2014].

Tetyukhina, D., 2010. High-resolution reservoir characterization by seismic inversion with geological constraints. p. 1.

Van Wagoner, J., 1985. Reservoir facies distribution as controlled by sea level changes. SEPM, Mid-Year Meeting, Golden, Colorado, Issue Abstracts with Program, pp. 91-92.

8. Appendix

8.1 Abbreviations

Well logs

- GR- Gamma ray
- NPHI- Neutron porosity
- RHOB- Density
- ILD- Deep resistivity
- MLSU- Medium resistivity
- SLFU- Shallow resistivity
- K- Permeability
- Sw- Water saturation
- SwInd- Indonesian Model Water saturation
- PhiDen- Density porosity
- VCLGR- Volume of clay

Modelling:

SGS - Sequential gaussian simulation

8.1.1 Appendix A Histograms

8.1.1.1 Well Ga-A3

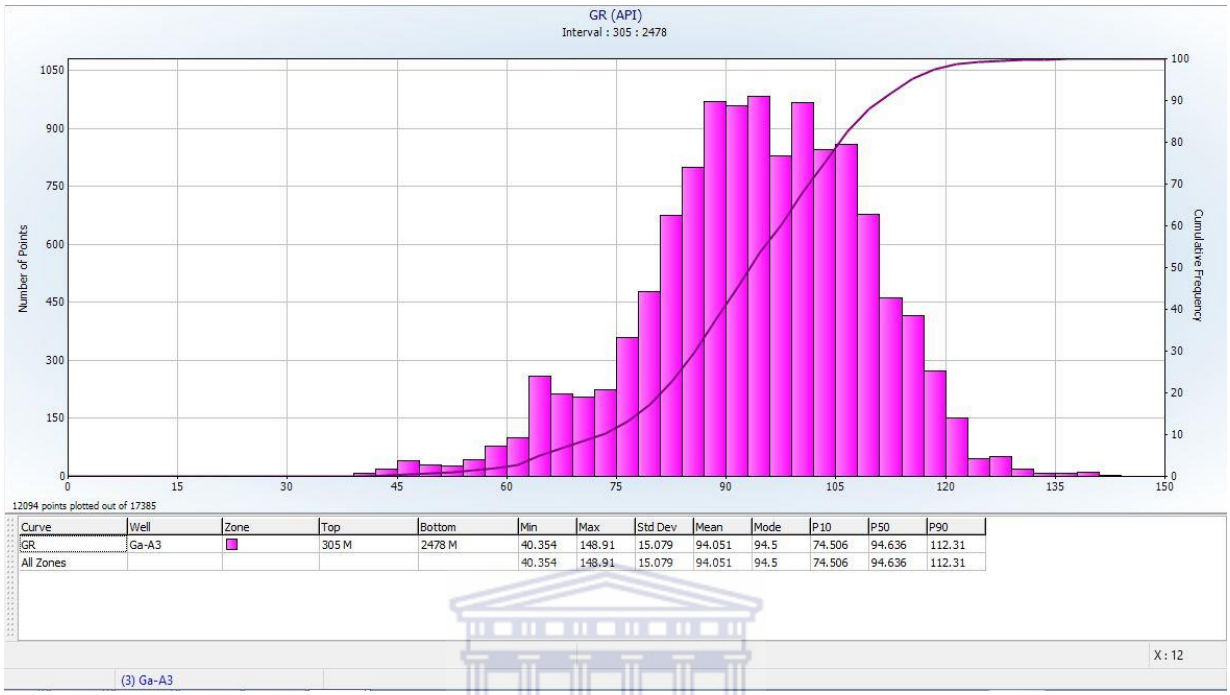

Curve	Well	Zone	Top	Bottom	Min	Max	Std Dev	Mean	Mode	P10	P50	P90
GR	Ga-A3		305 M	2478 M	40.354	148.91	15.079	94.051	94.5	74.506	94.636	112.31
All Zones					40.354	148.91	15.079	94.051	94.5	74.506	94.636	112.31

X : 12

(3) Ga-A3

8.1.1.2 Well Ga-Q1

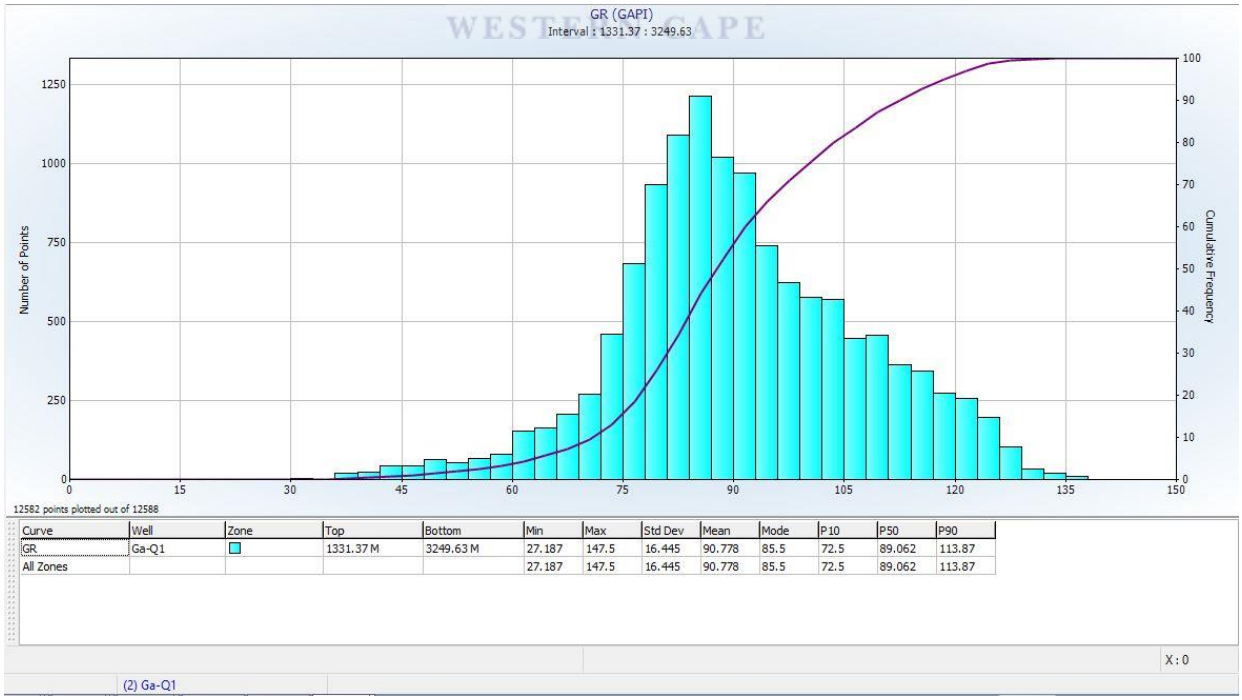

Curve	Well	Zone	Top	Bottom	Min	Max	Std Dev	Mean	Mode	P10	P50	P90
GR	Ga-Q1		1331.37 M	3249.63 M	27.187	147.5	16.445	90.778	85.5	72.5	89.062	113.87
All Zones					27.187	147.5	16.445	90.778	85.5	72.5	89.062	113.87

X : 0

(2) Ga-Q1

8.1.1.3 Well Ga-Q2

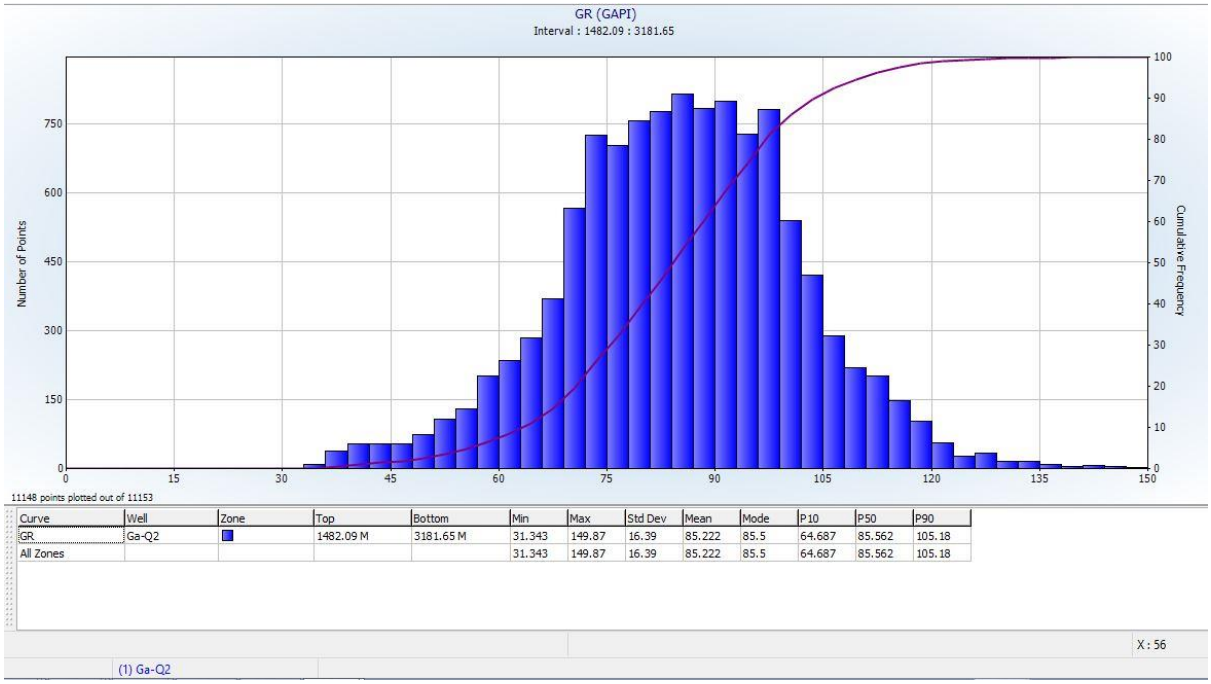

Curve	Well	Zone	Top	Bottom	Min	Max	Std Dev	Mean	Mode	P10	P50	P90
GR	Ga-Q2		1482.09 M	3181.65 M	31.343	149.87	16.39	85.222	85.5	64.687	85.562	105.18
All Zones					31.343	149.87	16.39	85.222	85.5	64.687	85.562	105.18

X : 56

(1) Ga-Q2

8.1.2 Appendix B: Cross plot of core analysis-regression function

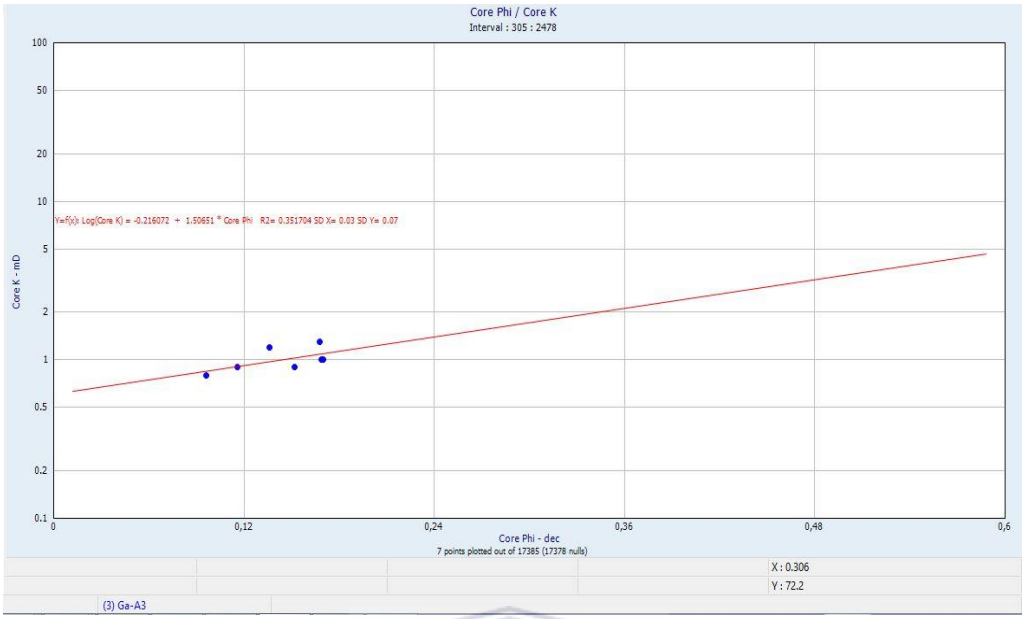

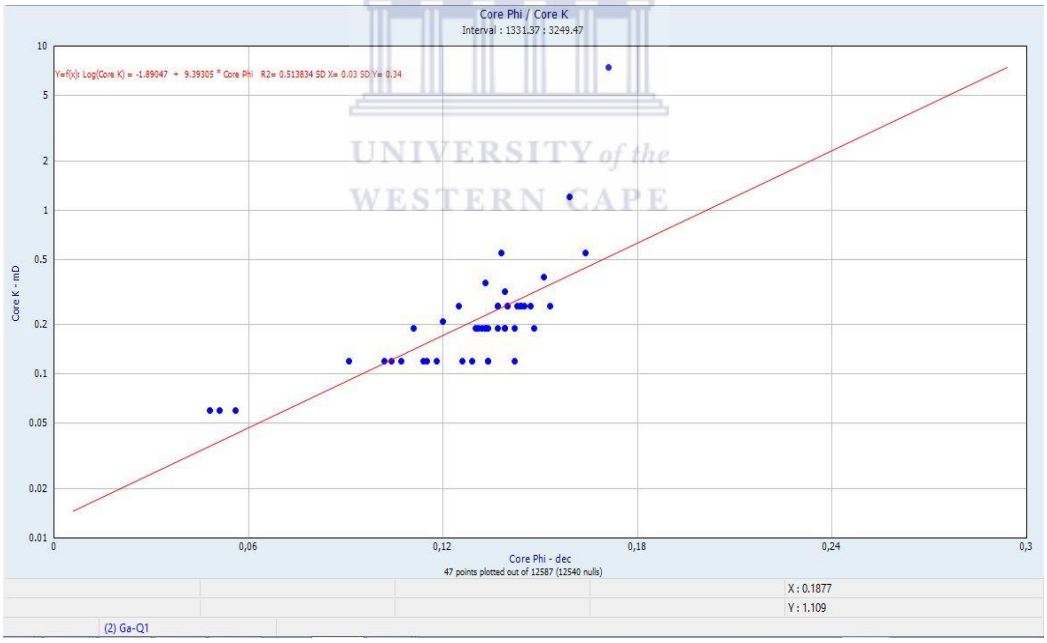

8.1.3 Appendix: Water Saturation parameters

Well Ga-A3				
Zone Name	**Top Depth**	**Bottom Depth**	**Parameter Clay volume(VCLGR)**	**Value**
Zone A	1649	1705	GR Clean – API	40.4
			GR Clay – API	144.7
Zone B	1734	1786	GR Clean – API	40.4
			GR Clay – API	144.7
Parameter- Porosity (PhiDen)				**Value**
RHO matrix – g/cc				2.65
RHO shale – g/cc				2.65
RHO water –g/cc				1.0
RHO gas – g/cc				0.2
Parameter- Sw				**Value**
Sat-Equation				Indonesia
Rw				0.1
a				1
m				2
n				2
Res Clay				1

Well Ga-Q1				
Zone Name	**Top Depth**	**Bottom Depth**	**Parameter Clay volume(VCLGR)**	**Value**
Zone A	2288	2348	GR Clean – API	27.2
			GR Clay – API	153.8
Zone B	2405	2455	GR Clean – API	27.2
			GR Clay – API	153.8
Parameter- Porosity (PhiDen)				**Value**
RHO matrix – g/cc				2.65
RHO shale – g/cc				2.75
RHO water –g/cc				1.0
RHO gas – g/cc				0.2
Parameter- Sw				**Value**
Sat-Equation				Indonesia
Rw				0.1
a				1
m				2
n				2
Res Clay				6.95

Well Ga-Q2				
Zone Name	**Top Depth**	**Bottom Depth**	**Parameter Clay volume(VCLGR)**	**Value**
Zone A	2261	2399	GR Clean – API	52
			GR Clay – API	89
Zone B	2416	2463	GR Clean – API	50
			GR Clay – API	105
Parameter- Porosity (PhiDen)				**Value**
RHO matrix – g/cc				2.65
RHO shale – g/cc				2.7
RHO water –g/cc				1.0
RHO gas – g/cc				0.2
Parameter- Sw				**Value**
Sat-Equation				Indonesia
Rw				0.1
a				1
m				2
n				2
Res Clay				7.8